J. Fluid Mech. (2012), *vol.* 707, *pp.* 150–190.
doi:10.1017/jfm.2012.268

Nonlinear interaction of wind-driven oblique surface waves and parametric growth of lower frequency modes

Sang Soo Lee†

Naval Surface Warfare Center, Carderock Division, West Bethesda, MD 20817, USA

(Received 14 July 2011; revised 17 May 2012; accepted 1 June 2012;
first published online 12 July 2012)

Nonlinear interactions between free-surface waves of the same wave speed and wind are studied by extending the linear resonant theory of Miles (*J. Fluid Mech.*, vol. 3, 1957, pp. 185–204). A nonlinear interaction can occur when the steepness of a primary three-dimensional wave, which propagates obliquely to the wind direction, becomes of the order of the cube of the density ratio of air to water. If a secondary wave of smaller amplitude is also an oblique wave, the nonlinear critical-layer interaction between the primary and secondary fluctuations in air generates a difference mode whose wavenumbers are equal to the differences between the primary and secondary values. In addition, the nonlinear interaction in the critical layer between the primary and difference modes induces a parametric-growth effect on the secondary surface wave, if the frequency of the primary wave is higher than that of the secondary wave. The primary wave remains linear during this '$2 + 1$ mode critical-layer interaction' stage between two free-surface waves and a nonlinearly generated mode. The evolution of the secondary-wave amplitude is governed by an integro-differential equation and that of the difference mode is determined by an integral equation. Both inviscid and viscous numerical results show that the nonlinear growth rates become much larger than the linear growth rates. Effect of viscosity is shown to delay the onset of the nonlinear growth. The growth of the secondary and difference modes is more effectively enhanced when the signs of propagation angles of the primary and secondary waves are opposite than when they are equal. The $2 + 1$ mode interaction can occur when wave steepnesses are very small. The nonlinear interaction is entirely confined to a thin critical layer, and the perturbations outside the critical layer are governed by linear equations. It is shown that the initial nonlinear growth of a free-surface wave could be governed by a mode–mode interaction in air.

Key words: critical layers, nonlinear instability, wind–wave interactions

1. Introduction

1.1. *Background*

A rational description of the energy transfer mechanism from wind to surface waves was given by Miles (1957). His theory describes how a resonant wind–wave interaction can be responsible for the energy transfer. This interaction occurs when the fluctuations in wind are synchronized with the motion of the air–water interface. The

† Email address for correspondence: SangSoo.Lee@navy.mil

growth of a surface wave is governed by the dynamics of air fluctuations with the air–water coupling at the interface. The critical layer plays an important role in this process by causing a phase jump of the fluctuation across the layer. The critical layer is a thin horizontal region surrounding the critical level where the mean wind velocity equals the wave speed in the wind direction. The quantity that is equal to frequency divided by streamwise wavenumber is referred to as the wave speed in the streamwise direction. Due to the critical-layer phase change, the peak of pressure fluctuation above the interface becomes out of phase with the crest of a wave and the surface wave becomes unstable. A small-steepness surface wave can grow exponentially according to Miles' (1957) theory. Its linear growth rate is of the order of the density ratio of air to water, whose typical value is $O(10^{-3})$.

A nonlinear interaction occurs when the surface-wave steepness becomes sufficiently large. However, its actual value does not have to be very large for an initial weakly nonlinear interaction. In fact, the nonlinear interaction of the present analysis takes place when the magnitude of wave steepness is as small as the cube of the density ratio of air to water, or $O(10^{-9})$. This indicates that nonlinear effects on the growth of wind-driven waves could be significant even in early stages of their evolution.

Fluctuations in air are governed by Rayleigh's stability equations and the unsteady flow in water is described by the potential flow solution, if the Reynolds number (based on characteristic wavelength and phase speed) is large and there is no mean motion in water. Since the wave growth rate is small, Rayleigh's stability equation has a singularity at the critical level at leading order. Nonlinear effects then first come into play in the critical layer (Benney & Bergeron 1969; Davis 1969; Drazin & Reid 2004). This nonlinear interaction is confined to the critical layer and the fluctuations outside the critical layer are still governed by linear dynamics. The critical layer in an early nonlinear stage of wave evolution is very thin. For example, the thickness of a non-equilibrium-type critical layer, where the wave growth effect is balanced with the mean-flow-convection effect, is of the order of the wave growth rate (Reutov 1980; Goldstein, Durbin & Leib 1987; Goldstein & Choi 1989; Lee & Wundrow 2011). The pressure and leading-order vertical velocity fluctuations can be shown to be constant across the critical layer, and amplitude equations can be obtained to describe the nonlinear evolution of wind-driven waves.

A nonlinear interaction of a two-dimensional surface wave, which travels along the wind direction, was studied by Reutov (1980). By using a matched asymptotic analysis, he showed that the nonlinear interaction first occurred in the critical layer when the wave steepness was of the order of the square of the density ratio of air to water. The evolution of a two-dimensional surface wave was governed by a system of equations that was analogous to those describing the nonlinear stage of instability of electrostatic waves in plasma. However, the nonlinear effect reduced the growth rate. The maximum amplitude of a surface wave was too small for the theory to be relevant for the ocean wave growth, as Reutov (1980) acknowledged. The strongly nonlinear critical-layer analyses of two-dimensional instability waves in an adverse-pressure-gradient boundary layer (Goldstein *et al.* 1987) and in free shear flows (Goldstein & Hultgren 1988; Hultgren 1992), and of two-dimensional wind-driven waves in strong gravitational astrophysical environments (Alexakis, Young & Rosner 2004*b*) discovered similar nonlinear critical-layer dynamics as in Reutov (1980).

In this study, we will instead focus our attention on the evolution of three-dimensional surface waves that propagate obliquely to the wind direction. A three-dimensional extension of Miles' (1957) linear theory shows that oblique surface waves can grow faster than their two-dimensional counterparts with the same wave speed in

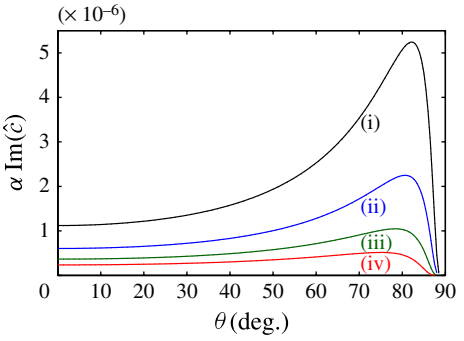

FIGURE 1. (Colour online) Linear growth rate $\alpha\,\mathrm{Im}(\hat{c})$ versus propagation angle θ for constant streamwise phase velocities: (black) curve (i), $c = 8$; (blue) curve (ii), $c = 10$; (green) curve (iii), $c = 12$; (red) curve (iv), $c = 14$. Equation (3.12) subject to (H 1)–(H 3) was numerically solved with (6.1) and (6.2) (except c). Quantities are normalized by friction velocity and roughness length as in (6.3).

the streamwise direction. Linear growth rates from numerical solutions of Rayleigh's stability equation with a logarithmic mean wind profile are plotted in figure 1. The oblique wave with a propagation angle of $\sim$80.5° has the largest growth rate when the wave speed, non-dimensionalized by friction velocity, is 10. It also shows that the growth rates of oblique waves with the same wave speed are comparable over a wide range of propagation angles, especially for the higher wave speeds considered. These inviscid linear results indicate that a three-dimensional wave, whose amplitude is at least comparable with that of a two-dimensional one, can exist in an initial wave field. We may have to include viscous and surface tension effects and solve the Orr–Sommerfeld equation for shorter waves with lower phase speeds (as in Valenzuela 1976; Blennerhassett 1980).

Unlike two-dimensional waves, nonlinear interactions of oblique Rayleigh instability waves can enhance their growth rates as shown by Goldstein & Choi (1989), Goldstein & Lee (1992), Wu (1992), Wu, Lee & Cowley (1993), Wundrow, Hultgren & Goldstein (1994), Goldstein (1995) and Lee (1997) in various shear flows. This enhanced growth can be continued or even accelerated during a series of subsequent nonlinear interaction stages. An initially thin critical layer becomes thicker as the growth rate is increased. The overall asymptotic structure of nonlinear critical-layer dynamics remains intact until the instability wave amplitude becomes $O(1)$ everywhere in a free shear layer (Goldstein & Lee 1993) or O(small wavenumber) in an adverse-pressure-gradient boundary layer (Goldstein & Lee 1992).

A nonlinear interaction in the critical layer can involve multiple modes provided they share the same critical layer or they have the same wave speed. Goldstein & Choi (1989) studied a multi-mode nonlinear interaction by considering a pair of oblique instability waves of a common phase speed, whose propagation angles had the same magnitude but opposite signs, in a free shear layer. They found that the nonlinear effect was driven by a cubic self-interaction of oblique modes. Amplitudes grew explosively and eventually became singular. The nonlinear interaction of a sub-harmonic resonant-triad of an equal phase speed, which is composed of a fundamental two-dimensional mode and a pair of sub-harmonic oblique modes with $\pm 60°$ propagation angles, was analysed by Goldstein & Lee (1992) in an adverse-pressure-gradient boundary layer and by Wu (1992) in the Stokes layer. Wu & Stewart

(1996) showed that the phase-locked interaction mechanism, as they termed it, could significantly relax the sub-harmonic resonance condition of previous studies. A two-dimensional instability mode can interact with an oblique mode, or a pair of oblique modes, of an arbitrary propagation angle, provided their wave speeds in the streamwise direction are equal. The wave speeds of the Rayleigh instability waves in shear flows are equal when their wavenumbers in their propagation directions are equal according to Squire's transformation (Drazin & Reid 2004). The phase-locked interaction of Wu & Stewart (1996) can occur in any shear flow which is inviscidly unstable. A multi-stage nonlinear interaction between the phase-locked triad of a two-dimensional and a pair of oblique Tollmien–Schlichting waves in boundary-layer transition was studied by Wu, Stewart & Cowley (2007). In both phase-locked and sub-harmonic resonant-triad interactions in incompressible flows, the two-dimensional mode was the most amplified linear mode that produced the initial nonlinear interaction. However, it was Goldstein & Choi's (1989) cubic self-interaction mechanism of oblique modes that caused the rapid growth of instability waves in a later nonlinear stage.

The linear critical-layer analysis of Miles (1957) is extended in this study to include nonlinear effects by using a matched asymptotic analysis. It will be shown that the nonlinear critical-layer interaction between unsteady fluctuations in air, which are synchronized with free-surface waves, is responsible for the faster than exponential growth of free-surface waves. Because of the leading-order singularity of Rayleigh's instability equation, a nonlinear interaction can first occur in the critical layer, as shown by Reutov (1980) and others. Our analysis describes how this nonlinear critical-layer interaction gradually evolves from the interaction between linear free-surface waves with small steepnesses. A three-dimensional primary wave, which travels obliquely to the wind direction, is assumed to be identifiable in an initial linear wave field. Once this primary wave becomes sufficiently large, the nonlinear critical-layer interaction starts to affect the growth of a secondary oblique wave that also grows linearly in the initial stage. If their wave speeds in the streamwise direction are equal, they share the common critical layer where their localized nonlinear interaction occurs. The frequency or propagation angle of the secondary wave, whose amplitude is smaller than the primary one, can be arbitrarily chosen. Though it is the largest oblique wave, the primary wave is not required to be larger than a two-dimensional wave that propagates along the wind direction. It can be shown that the present nonlinear interaction between oblique waves is not affected by a two-dimensional wave if the steepness of the latter is smaller than the order of the square of the density ratio of air to water. The exponentially growing two-dimensional wave remains passive even though it may be the largest. Although it plays an active role in enhancing the growth rate of a smaller secondary wave, the primary wave also remains linear in this early nonlinear stage.

With large Reynolds numbers, the viscosity effect only enters the critical-layer equations. Although the analysis is developed for free-surface waves with an arbitrary wind profile, it is assumed that the curvature of wind profile at the critical level is $O(1)$. The existence and relevance of the critical-layer dynamics of gravity waves in nature were found by Hristov, Miller & Friehe (2003). By using a linear filter to identify the wave-induced air fluctuations from the measured wind velocities and wave elevations over the open ocean, they were able to clearly identify the critical-layer dynamics. They showed that there was a good agreement between the measured and theoretical (Miles 1957) fluctuation velocities. Janssen (2004) also reasoned that Miles' (1957) mechanism seemed to provide an adequate model for the growth of surface waves.

Although we will present our analysis in the context of water waves, it can be applied to the wind–wave interaction in astrophysical environments where the gravity becomes strong and density ratio becomes finite. Alexakis *et al.* (2004*b*) showed that their nonlinear analysis of a two-dimensional wave in the large gravity limit becomes essentially the same as that of Reutov (1980) developed in the small density limit. It has been observed, from references quoted before, that the nonlinear critical-layer analyses in various shear flows produce the same amplitude equations.

Underlying physics of the localized nonlinear interaction, occurring in their common critical layer, between wave-synchronized fluctuations is straightforward. Furthermore, the final amplitude equations and their analytic solutions are also fairly simple. The analysis, however, turns out to be pretty complex because it involves three modes of different characteristics. Moreover, in this analysis, the leading-order outer solutions are affected by the nonlinear critical-layer dynamics through the boundary conditions on the edges of the critical layer while they are still governed by linear equations. In order to simplify the outer solutions, some functional forms of the nonlinear interaction results are assumed to be known in the earlier parts of the paper, causing the analysis to be more involved. The references to the subsequent parts of the manuscript are provided to reduce possible ambiguities and can be ignored during the first time reading.

The mechanism of the nonlinear critical-layer interaction will be presented in the following § 1.2, and the formulation of the problem will be given in § 2. The analysis of the unsteady flow outside the critical layer will be given in § 3 with that inside the critical layer in § 4. In § 5, the critical-layer equations will be analytically solved and they will be matched with the outer solutions to derive amplitude equations. Final amplitude equations will be presented in §§ 5.2 and 5.3 with complete references for the parameters appearing in them. The analytic solutions of amplitude equations will be given in § 5.5, and their numerical evaluation will be presented in § 6. The summary of the analysis will be presented in § 7.

1.2. $2+1$ *mode critical-layer interaction*

The wave speed of an oblique surface wave, of which the velocity potential is proportional to $\exp[\mathrm{i}\alpha(x-ct)+\mathrm{i}\beta y]$, is related to the wavenumbers by the free-surface-wave dispersion relation, $c^2=(G\gamma/\alpha^2)\tanh(\gamma H)$, as in (3.22), where $\mathrm{i}\equiv\sqrt{-1}$, $\gamma\equiv\sqrt{\alpha^2+\beta^2}$, α and β are the streamwise and spanwise wavenumbers, c is the wave speed in the streamwise direction, H is the depth of water, and G is the gravity parameter defined in (2.4). The lateral spanwise direction in y is perpendicular to the streamwise wind direction in x as shown in figure 2. All quantities are non-dimensionalized by characteristic length and velocity scales (see § 2). A contour line of a constant wave speed c in the (α,β) plane is plotted as the solid curve in figure 3. Note that the frequency ($\omega=\alpha c$) of a two-dimensional wave travelling along wind direction, denoted by the letter S_o, is lower than those of obliquely propagating three-dimensional waves, in contrast to those of the Rayleigh instability waves in free shear flows and boundary layers. As a result, the nonlinear critical-layer interaction between a two-dimensional and oblique waves does not occur for the free-surface waves (cf. Wu & Stewart 1996).

It is assumed that a primary three-dimensional surface wave, denoted by the letter P in figure 3, can be identified as the largest oblique one in an initial wave field (where a larger two-dimensional wave can coexist: see § 7). Its velocity potential is proportional to $\exp[\mathrm{i}\alpha_p(x-ct)+\mathrm{i}\beta_p y]$. The velocity potential of a secondary wave of smaller amplitude, denoted by the letter S, is proportional to $\exp[\mathrm{i}\alpha_s(x-ct)+\mathrm{i}\beta_s y]$.

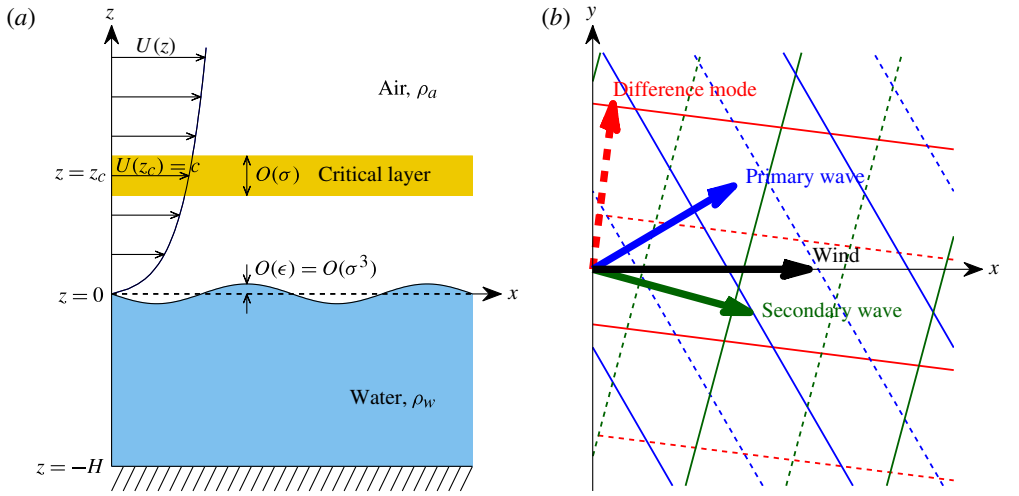

FIGURE 2. (Colour online) Schematic diagram of a flow field. A right-handed Cartesian coordinate system (x, y, z) is attached to the calm-water surface. In (a) the y-axis is pointing into the page, and in (b) the z-axis is pointing out of the page. The critical layer of $O(\sigma)$ thickness is located at $z = z_c$, where $U(z_c)$ is equal to the wave speed c. The wave elevations are of $O(\epsilon)$ for the primary wave, $O(\epsilon\delta)$ for the secondary wave, and $O(\sigma\epsilon\delta)$ for the difference mode, where $\sigma \equiv \rho_a/\rho_w$ is the density ratio, $\epsilon = \sigma^3$ and $\delta \ll 1$, as in (2.1), (4.5) and (4.6). In (b), the depicted wave propagation angles are $\theta_p = 30°$, $\theta_s = -15°$ and $\theta_d = 82.8°$, for the primary, secondary and difference modes, with θ_t defined by (3.7). The wavenumber vector of the difference mode was plotted as a dotted arrow because it does not satisfy the free-surface-wave dispersion relation. The wave crests are plotted as solid lines and troughs as dotted lines.

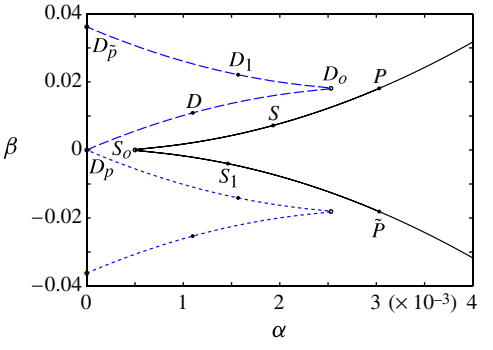

FIGURE 3. (Colour online) Diagram of the $2 + 1$ mode critical-layer interaction in the (α, β) coordinates. The primary and secondary modes are located on the black solid curve that depicts the free-surface-wave dispersion relation (3.22) when $c = 10$, $G = 0.05$ and $H = 10^{35}$. The primary mode P and the secondary mode S or S_1 (or any one on the section $P \to S_o \to \tilde{P}$) generate the difference mode D or D_1 (or one on the blue dashed curve $D_p \to D_o \to D_{\tilde{p}}$). The primary mode $\tilde{P}$ and a secondary mode on $P \to S_o \to \tilde{P}$ generate a difference mode on the (blue) dotted curve.

A nonlinear interaction between these two initially linear waves first occurs in their common critical layer when the primary-wave steepness becomes of the order of the cube of the density ratio (see § 4).

The nonlinear critical-layer interaction between the primary and secondary fluctuations in air, which are synchronized with the corresponding free-surface waves, generates a difference mode, which is proportional to $\exp[\mathrm{i}(\alpha_p-\alpha_s)(x-ct)+\mathrm{i}(\beta_p-\beta_s)y]$ and denoted by the letter D in figure 3. Its amplitude becomes as large as the secondary-mode amplitude in air, but smaller than the latter in water if the difference mode does not satisfy the free-surface-wave dispersion relation (see appendix A). Also, the nonlinear coupling between the primary and difference modes, which occurs within the critical layer, induces a nonlinear growth of the secondary free-surface wave, if the primary frequency ω_p $(=\alpha_p c)$ is higher than the secondary one ω_s $(=\alpha_s c)$, or $\alpha_p > \alpha_s$. During the whole stage, the primary wave remains linear. This interaction involves two free-surface waves and one nonlinearly generated mode, and might be termed the '2+1 mode critical-layer interaction' (cf. the three-wave resonance interaction of Phillips 1960). As the arbitrarily chosen secondary wave moves from $P \to S_o \to \tilde{P}$ on the solid curve in figure 3, the corresponding difference mode moves from $D_p \to D_o \to D_{\tilde{p}}$ on the dashed curve. The difference modes on the dotted curve are generated by the primary wave $\tilde{P}$ interacting with the secondary waves on $P \to S_o \to \tilde{P}$. The dynamics of this $2+1$ mode interaction are similar to those of the phase-locked interaction of Wu & Stewart (1996). But the role of their two-dimensional mode is now replaced by the primary oblique wave.

2. Formulation

A right-handed Cartesian coordinate system (x, y, z) with unit vectors $(\boldsymbol{i}, \boldsymbol{j}, \boldsymbol{k})$ is attached to the calm-water surface with x in the streamwise direction of the wind, y in the spanwise lateral direction, and z in the vertical transverse direction pointing up, as shown in figure 2. We suppose that the mean flow in air is two-dimensional and there is no mean motion in water.

It is assumed that there are three-dimensional linear waves propagating obliquely to the wind direction in an initial wave field. The largest oblique wave is referred to as the 'primary wave'. A secondary oblique wave can be arbitrarily chosen as long as its wave speed is equal to that of the primary one. Its wave elevation is smaller than the primary one. The streamwise wavenumber (or frequency) of the secondary oblique wave is assumed to be smaller than the primary one for the 2+1 mode interaction. The common wave speed is supposed to be smaller than the maximum wind speed. Both waves grow exponentially in the initial small-steepness stage due to Miles' (1957) resonance mechanism. Once the primary-wave steepness becomes sufficiently large, a nonlinear effect will enhance the growth of the secondary wave. If the magnitude of a two-dimensional wave that propagates in the wind direction is smaller than the order of the square of the density ratio of air to water, it will not affect the present nonlinear interaction between oblique waves even though it is larger than the primary wave.

The water is taken to be bounded from below by a fixed horizontal plane at $z = -H$. Most of the analysis is valid for an arbitrary H, except for the difference-mode amplitude equation in § 5, which is written for the case where the free-surface-wave dispersion relation is not satisfied by the difference mode (see appendix A). As in Miles (1957), the air turbulence effect is not separately included. All lengths, velocities, pressures and time in both fluid flows are non-dimensionalized by Δ_a, U_a, $\rho_a U_a^2$ and Δ_a/U_a, where Δ_a and U_a are characteristic length and velocity scales of

the air flow. For the present analysis, the wavelength and wave speed of the primary wave could be a proper choice for Δ_a and U_a, respectively. The Reynolds numbers, based on Δ_a and U_a, are assumed to be large, so the viscosity effect only enters the critical-layer equations. The surface tension effect is not included in this study.

The air and water are assumed incompressible and the ratio of densities is defined as

$$\rho_a/\rho_w = \sigma, \tag{2.1}$$

where the subscripts a and w denote the quantities of air and water, respectively, and $\sigma \ll 1$ characterizes the small density ratio of air to water.

Perturbation to the air–water interface about the calm-water surface, $z = 0$, is described by

$$z = \epsilon\tilde{h}(x, y, t), \tag{2.2}$$

where ϵ is a measure of a wave steepness and $\tilde{h}$ is a scaled wave elevation. The scaling relation between ϵ and σ will be determined in § 4 by the dynamics in the critical layer, which surrounds the critical level at which the mean velocity is equal to the wave speed in the streamwise direction or to the frequency divided by streamwise wavenumber (see § 3.1). The scaling is obtained so that the present analysis can describe the nonlinear dynamics of wave interaction that gradually evolve from the interaction of initially linear surface waves with small steepnesses. Nonlinear effects in the resulting equations will become negligibly small in the initial stage, and they will reduce to the linear equations of Miles (1957).

The total velocity $\boldsymbol{u} = \boldsymbol{i}u + \boldsymbol{j}v + \boldsymbol{k}w$ and pressure p in air are composed of a steady wind and mean pressure plus wave-induced perturbations $\tilde{\boldsymbol{u}} = \boldsymbol{i}\tilde{u} + \boldsymbol{j}\tilde{v} + \boldsymbol{k}\tilde{w}$ and $\tilde{p}$,

$$\boldsymbol{u} = \boldsymbol{i}U(z) + \epsilon\tilde{\boldsymbol{u}}(\boldsymbol{x}, t), \quad p = P_0 - Gz + \epsilon\tilde{p}(\boldsymbol{x}, t), \tag{2.3}$$

where $U(z)$ is the mean wind velocity and P_0 denotes the non-dimensional mean reference pressure at the calm-water surface. The parameter

$$G \equiv \mathrm{g}\Delta_a/U_a^2 \tag{2.4}$$

measures the ratio of the potential energy associated with surface waves to the kinetic energy in the wind, where g denotes the acceleration due to gravity. It is assumed that the mean velocity at the air–water interface is continuous, i.e. in this case

$$U(0) = 0, \tag{2.5}$$

and the effect of the Kelvin–Helmholtz instability is not included. Although the usual logarithmic wind profile will be chosen for the numerical results presented in § 6, the analysis will be carried out for an arbitrary mean velocity without an inflection point. It is also assumed that the critical layer is distinct from the viscous sublayer of the mean flow so that the curvature of wind profile is $O(1)$ at the critical level.

Governing equations for the wave-induced fluctuations become, for $z > \epsilon\tilde{h}$,

$$\nabla \cdot \tilde{\boldsymbol{u}} = 0, \quad \tilde{\boldsymbol{u}}_t + U\tilde{\boldsymbol{u}}_x + \boldsymbol{i}U_z\tilde{w} + \epsilon\tilde{\boldsymbol{u}} \cdot \nabla\tilde{\boldsymbol{u}} = -\nabla\tilde{p} + R_a^{-1}\nabla^2\tilde{\boldsymbol{u}}, \tag{2.6}$$

where $R_a = U_a\Delta_a/\nu_a$ with ν_a denotes the kinematic viscosity of air. An independent variable used as a subscript denotes a derivative with respect to that variable. The fluctuations in air must decay at the upper boundary, i.e. $\tilde{\boldsymbol{u}}, \tilde{p} \to 0$ as $z \to \infty$.

Since there is no current, the fluid motion in water is solely due to the presence of the surface waves and so is irrotational. The solution for $z < \epsilon\tilde{h}$ can be expressed as

$$\boldsymbol{u} = \epsilon\nabla\tilde{\phi}(\boldsymbol{x}, t), \quad p = P_0 - (1/\sigma)Gz + (\epsilon/\sigma)\tilde{p}_w, \tag{2.7}$$

where the velocity potential $\tilde{\phi}$ satisfies $\nabla^2\tilde{\phi}=0$, subject to the boundary condition $\tilde{\phi}_z=0$ at $z=-H$. The perturbed pressure in the water can be expressed in terms of the velocity potential by $\tilde{p}_w=-\tilde{\phi}_t-\epsilon(1/2)\nabla\tilde{\phi}\cdot\nabla\tilde{\phi}$.

Motions of air and water are coupled through conditions at the interface defined by (2.2). The kinematic condition requires that the interface be a material surface for both fluid flows, and therefore

$$\boldsymbol{u}\cdot\nabla(z-\epsilon\tilde{h})=\epsilon\tilde{h}_t \quad \text{at } z=\epsilon\tilde{h}_+, \qquad \nabla\tilde{\phi}\cdot\nabla(z-\epsilon\tilde{h})=\tilde{h}_t \quad \text{at } z=\epsilon\tilde{h}_-, \tag{2.8}$$

where $\tilde{h}_+$ and $\tilde{h}_-$ denote the air and water sides of the interface, respectively. The dynamic condition at the interface requires that the pressure there be continuous. This can be satisfied if the pressure changes in the streamwise and spanwise directions on the water surface, $(p_x+\epsilon\tilde{h}_x p_z)/\left(1+\epsilon^2\tilde{h}_x^2\right)^{1/2}$ and $(p_y+\epsilon\tilde{h}_y p_z)/\left(1+\epsilon^2\tilde{h}_y^2\right)^{1/2}$ are equal on both sides (Wehausen & Laitone 1960). The dynamic condition becomes

$$\sigma\,[\tilde{p}_x-(G-\epsilon\tilde{p}_z)\tilde{h}_x]_{z=\epsilon\tilde{h}_+}=[\tilde{p}_{wx}-(G-\epsilon\tilde{p}_{wz})\tilde{h}_x]_{z=\epsilon\tilde{h}_-}, \tag{2.9a}$$

$$\sigma\,[\tilde{p}_y-(G-\epsilon\tilde{p}_z)\tilde{h}_y]_{z=\epsilon\tilde{h}_+}=[\tilde{p}_{wy}-(G-\epsilon\tilde{p}_{wz})\tilde{h}_y]_{z=\epsilon\tilde{h}_-}\,. \tag{2.9b}$$

3. Unsteady flow outside the critical layer

The unsteady flow in the outer region is composed of the primary, secondary and difference modes. The difference oblique mode in this region is induced by the nonlinear critical-layer interaction, which produces its velocity jump across the layer. Its wave speed is equal to that of the primary and secondary oblique waves. In an attempt to reduce confusion, the term 'wave' will be used to denote the surface wave, 'fluctuation' for the perturbation in air, and 'mode' to cover both fluid flows.

3.1. *Unsteady flow in water*

The velocity potential $\tilde{\phi}$ and pressure perturbation $\tilde{p}_w$ in water and the interface surface elevation $\tilde{h}$ can be written as, in the limit $\sigma\to 0$,

$$\begin{pmatrix}\tilde{\phi}\\ \tilde{p}_w\\ \tilde{h}\end{pmatrix}=\tilde{B}_p\begin{pmatrix}\hat{\phi}_p^{(1)}+\sigma\hat{\phi}_p^{(2)}\\ \hat{p}_p^{(1)}+\sigma\hat{p}_p^{(2)}\\ \hat{h}_p^{(1)}+\sigma\hat{h}_p^{(2)}\end{pmatrix}\mathscr{E}_p+\delta\tilde{B}_s\begin{pmatrix}\hat{\phi}_s^{(1)}+\sigma\hat{\phi}_s^{(2)}\\ \hat{p}_s^{(1)}+\sigma\hat{p}_s^{(2)}\\ \hat{h}_s^{(1)}+\sigma\hat{h}_s^{(2)}\end{pmatrix}\mathscr{E}_s$$
$$+\sigma\delta\tilde{B}_d\begin{pmatrix}\hat{\phi}_d^{(2)}\\ \hat{p}_d^{(2)}\\ \hat{h}_d^{(2)}\end{pmatrix}\mathscr{E}_d+\text{c.c.}+\cdots, \tag{3.1}$$

where c.c. denotes the complex conjugate, $\mathrm{i}\equiv\sqrt{-1}$, and

$$\mathscr{E}_p\equiv\mathrm{e}^{\mathrm{i}(\alpha_p X+\beta_p y)}, \quad \mathscr{E}_s\equiv\mathrm{e}^{\mathrm{i}(\alpha_s X+\beta_s y)}, \quad \mathscr{E}_d\equiv\mathrm{e}^{\mathrm{i}(\alpha_d X+\beta_d y)}. \tag{3.2}$$

The quantities of the primary, secondary and difference modes are denoted by the subscripts p, s and d, respectively. The magnitude of the unscaled wave elevation $\epsilon\tilde{h}$ is $O(\epsilon)$ for the primary wave and $O(\epsilon\delta)$ for the secondary wave. The ϵ is a measure of the steepness of the primary surface wave and δ is a measure of the amplitude ratio of the secondary to primary waves. The scalings of ϵ and δ will be determined later by (4.5) and (4.6). The magnitude of the difference-mode wave elevation becomes $O(\sigma\epsilon\delta)$

since we only consider the case, for simplicity, where the difference mode does not satisfy the free-surface-wave dispersion relation.

The time scale over which the wave growth occurs becomes

$$t_1 \equiv \sigma t, \tag{3.3}$$

and the normalized streamwise coordinate X in a reference frame moving with the common c is given by

$$X \equiv x - ct. \tag{3.4}$$

The scaling for the slow time t_1 is determined by the magnitude of linear growth rates of the primary and secondary surface waves, which is $O(\sigma)$ (Miles 1957). The amplitude functions that account for the slow growth of waves are denoted by $\tilde{B}_\iota(t_1)$ for $\iota = \{p, s, d\}$.

The spanwise wavenumbers β_p and β_s of the primary and secondary waves, respectively, can be positive or negative as illustrated in figure 3. The primary streamwise wavenumber, α_p, is assumed to be larger than the secondary one, α_s,

$$0 < [\alpha_{2D}] < \alpha_s < \alpha_p. \tag{3.5}$$

Then the frequency of the primary wave, ω_p $(=\alpha_p c)$, is higher than the secondary frequency, ω_s $(=\alpha_s c)$. The case when ω_s is larger than ω_p will be considered in a separate analysis. Since both primary and secondary waves start out as linear surface waves, they satisfy the free-surface-wave dispersion relations that will be derived later in (3.22). The relation for a two-dimensional surface wave becomes $\alpha_{2D}/\tanh(\alpha_{2D}H) = G/c^2$. Since its left-hand side is larger than $1/H$, a two-dimensional wave does not exist if $c^2 > GH$, and $[\alpha_{2D}]$ in (3.5) is written with square brackets. The streamwise and spanwise wavenumbers of the difference mode, α_d and β_d, respectively, become

$$\alpha_d = \alpha_p - \alpha_s, \quad \beta_d = \beta_p - \beta_s, \tag{3.6}$$

where $\alpha_d > 0$, but β_d can be positive or negative depending on the values of β_p and β_s. It is shown in appendix A that, for a given c, α_d and β_d do not satisfy the free-surface-wave dispersion relation except in the shallow water limit with $\beta_p\beta_s > 0$.

The $c\,(=\omega_\iota/\alpha_\iota)$ in (3.4), that is equal to the frequency divided by streamwise wavenumber, is the wave speed in the streamwise direction (Drazin & Reid 2004, p. 128). If the wavenumber in the propagation direction, γ_ι, and the wave propagation angle with respect to wind direction, θ_ι, are defined by

$$\gamma_\iota \equiv \sqrt{\alpha_\iota^2 + \beta_\iota^2}, \quad \theta_\iota = \arctan(\beta_\iota/\alpha_\iota), \tag{3.7}$$

for $\iota = \{p, s, d\}$, the phase speed in the wave direction $\bar{c}_\iota$ $(=\omega_\iota/\gamma_\iota)$ becomes

$$\bar{c}_\iota = c\,\cos\theta_\iota. \tag{3.8}$$

The expressions (3.1)–(3.4) represent oblique waves which travel in the direction $(\alpha_\iota, \beta_\iota)$ with phase speed $\bar{c}_\iota$. It is worth noticing that c is larger than $\bar{c}_\iota$. Thus, the critical layer of an oblique wave is always located at a greater height than that of a two-dimensional wave with an equal phase speed $\bar{c}_\iota$. For an oblique wave with the same $\bar{c}_\iota$, the location of the critical layer moves away from the interface, or from the viscous sublayer, as θ_ι is increased. Meanwhile, for the same c, the phase speed $\bar{c}_\iota$ becomes lower and the wavelength becomes shorter for an oblique wave with larger θ_ι.

From (3.1), we find that both leading-order and second-order velocity potentials, $\hat{\phi}_\iota^{(1)}(z)$ and $\hat{\phi}_\iota^{(2)}(z,t_1)$, satisfy the Laplace equation, i.e. for $\iota=\{p,s,d\}$ and $\ell=\{1,2\}$,

$$(\partial_z^2-\gamma_\iota^2)\hat{\phi}_\iota^{(\ell)}=0,\quad \text{subject to } \partial_z\hat{\phi}_\iota^{(\ell)}=0 \quad \text{at } z=-H, \tag{3.9}$$

where $\partial_z\equiv\partial/\partial z$. The t_1-dependence of $\hat{\phi}_\iota^{(2)}(z,t_1)$ was included to facilitate the matching with the fluctuations in air.

The pressure components $\hat{p}_\iota^{(1)}(z)$ and $\hat{p}_\iota^{(2)}(z,t_1)$ in (3.1) can be written as

$$\hat{p}_\iota^{(1)}=\mathrm{i}\alpha_\iota c\hat{\phi}_\iota^{(1)},\quad \hat{p}_\iota^{(2)}=\mathrm{i}\alpha_\iota c\hat{\phi}_\iota^{(2)}-(\tilde{B}_\iota'/\tilde{B}_\iota)\hat{\phi}_\iota^{(1)} \tag{3.10}$$

where the prime denotes the differentiation with respect to the relevant argument, i.e. $\tilde{B}_\iota'\equiv \mathrm{d}\tilde{B}_\iota/\mathrm{d}t_1$.

3.2. *Unsteady flow in air*

Fluctuations in air outside the critical layer are also governed by linear equations to the required order of approximation. The velocity and pressure field can be written as, in the limit $\sigma\to 0$,

$$\begin{pmatrix} u-U\\ v\\ w\\ p-P_0+Gz\end{pmatrix}=\epsilon\tilde{B}_p\begin{pmatrix}\hat{U}_p\\ \hat{V}_p\\ -\mathrm{i}\gamma_p\Phi_p\\ \Pi_p\end{pmatrix}\mathscr{E}_p+\epsilon\delta\tilde{B}_s\begin{pmatrix}\hat{U}_s\\ \hat{V}_s\\ -\mathrm{i}\gamma_s\Phi_s\\ \Pi_s\end{pmatrix}\mathscr{E}_s$$
$$+\epsilon\delta\tilde{B}_d\begin{pmatrix}\hat{U}_d\\ \hat{V}_d\\ -\mathrm{i}\gamma_d\Phi_d\\ \Pi_d\end{pmatrix}\mathscr{E}_d+\text{c.c.}+\cdots. \tag{3.11}$$

The magnitude of velocity and pressure fluctuations in air is $O(\epsilon)$ for the primary mode, and $O(\epsilon\delta)$ for the secondary and difference modes.

The shape functions, $\Phi_p(z)$, $\Phi_s(z,t_1)$ and $\Phi_d(z,t_1)$, satisfy Rayleigh's stability equation to the required levels of approximation, for $\iota=\{p,s,d\}$,

$$(U-\hat{c}_\iota)(\partial_z^2-\gamma_\iota^2)\Phi_\iota-U''\Phi_\iota=0, \tag{3.12}$$

where $U''\equiv \mathrm{d}^2U/\mathrm{d}z^2$ and the complex $\hat{c}_\iota$ is defined by

$$\hat{c}_\iota=c+\sigma\mathrm{i}\tilde{B}_\iota'/(\alpha_\iota\tilde{B}_\iota). \tag{3.13}$$

The decaying boundary condition at the upper boundary becomes $\Phi_\iota\to 0$ as $z\to\infty$. The scaled shape functions $\hat{U}_\iota$, $\hat{V}_\iota$ and Π_ι become

$$\{\hat{U}_\iota,\ \hat{V}_\iota\}=\{\tan\theta_\iota,\ -1\}\,(\sin\theta_\iota)U'\Phi_\iota/(U-\hat{c}_\iota)+\{\cos\theta_\iota,\ \sin\theta_\iota\}\,\partial_z\Phi_\iota+\cdots, \tag{3.14}$$

$$\Pi_\iota=-(U-\hat{c}_\iota)(\cos\theta_\iota)\hat{V}_\iota+\cdots. \tag{3.15}$$

Since the primary mode remains linear throughout the entire analysis, $\Phi_p(z)$ only depends on z. However, $\Phi_s(z,t_1)$ and $\Phi_d(z,t_1)$ for the secondary and difference modes become dependent on t_1 because of the nonlinear effects, as will be shown below by (3.25) and (B 8). The nonlinear jump across the critical layer, which is a function of the slow time t_1, occurs at leading order in this analysis. Thus, the nonlinear critical-layer effect must be included in the leading-order outer solution. This is different

from the weakly nonlinear analyses of the instability waves in shear flows where the critical-layer jump occurs at higher order (Goldstein *et al.* 1987; Goldstein & Hultgren 1988; Goldstein & Choi 1989).

3.3. *Interface conditions*

By substituting (2.7), (3.1) and (3.11) into the kinematic and dynamic interface conditions (2.8) and (2.9) and by expanding the results about the calm-water interface, we obtain the interface conditions at $z = 0$,

$$\begin{pmatrix} \hat{h}_\iota^{(1)} \\ \hat{h}_\iota^{(2)} \end{pmatrix} = \frac{\mathrm{i}}{\alpha_\iota c} \begin{pmatrix} \partial_z \hat{\phi}_\iota^{(1)} \\ \partial_z \hat{\phi}_\iota^{(2)} \end{pmatrix} + \begin{pmatrix} 0 \\ (\partial_z \hat{\phi}_\iota^{(1)}) \tilde{B}_\iota' / (\alpha_\iota^2 c^2 \tilde{B}_\iota) \end{pmatrix}, \quad \hat{h}_\iota^{(1)} = \frac{\gamma_\iota}{\alpha_\iota c} \Phi_\iota, \tag{3.16}$$

$$\left(G\partial_z - \alpha_\iota^2 c^2\right) \begin{pmatrix} \hat{\phi}_\iota^{(1)} \\ \hat{\phi}_\iota^{(2)} \end{pmatrix} = \begin{pmatrix} 0 \\ \alpha_\iota^2 c^2 \left[1 + 2\mathrm{i}\tilde{B}_\iota' / (\alpha_\iota c \tilde{B}_\iota)\right] \hat{\phi}_\iota^{(1)} + (\mathrm{i}\alpha_\iota^2 c / \gamma_\iota)(U_0' + c\,\partial_z)\Phi_\iota \end{pmatrix}, \tag{3.17}$$

where

$$U_0' \equiv U'(z = 0). \tag{3.18}$$

From the leading-order kinematic interface condition in (3.16), one can find that

$$\Phi_\iota = (\mathrm{i}/\gamma_\iota)\, \partial_z \hat{\phi}_\iota^{(1)} \quad \text{at } z = 0, \tag{3.19}$$

which can be viewed as a normalization condition for Φ_p and Φ_s.

For the primary and secondary waves, the leading-order potentials in water $\hat{\phi}_p^{(1)}$ and $\hat{\phi}_s^{(1)}$ are not affected by the wind. These leading-order potentials can induce the corresponding fluctuations in air via the kinematic condition (3.19). The wave growth rates are determined by using the second-order dynamic condition in (3.17). For the difference mode, the nonlinearly generated fluctuation in air by critical-layer interaction induces the second-order potential in water $\hat{\phi}_d^{(2)}$ through the second-order dynamic condition in (3.17). Its leading-order potential in water $\hat{\phi}_d^{(1)}$ is zero.

3.4. *Outer solution of the secondary mode*

For the Rayleigh equation (3.12) of the secondary and difference modes, the boundary conditions on the edges of the critical layer are affected by nonlinear critical-layer interactions. Since those of the secondary mode include both linear and nonlinear effects, its outer solution will be presented first. The outer solution of the difference mode only includes the nonlinear effect and that of the primary mode only includes the linear effect. They will be given in §§ B.1 and B.2 as subsets of the secondary-mode solution.

The velocity potentials in the water, $\hat{\phi}_s^{(1)}$ and $\hat{\phi}_s^{(2)}$ become

$$\hat{\phi}_s^{(1)} = \cosh\left[\gamma_s(z + H)\right] / \cosh(\gamma_s H), \quad \hat{\phi}_s^{(2)} = 0, \tag{3.20}$$

where they are normalized by

$$\hat{\phi}_s^{(1)} + \sigma \hat{\phi}_s^{(2)} = 1 \quad \text{at } z = 0. \tag{3.21}$$

The above solution is acceptable because the left-hand side of the second-order equation in (3.17) will always be zero for any choice of $\hat{\phi}_s^{(2)}$. The free-surface-wave

dispersion relation is obtained from the first equation in (3.17) as

$$c^2 = \left(G\gamma_s/\alpha_s^2\right)\tanh(\gamma_s H), \quad \text{or } \beta_s^2/\alpha_s^2 = c^4\alpha_s^2/[G^2\tanh^2(\gamma_s H)] - 1. \tag{3.22}$$

By putting (3.20) into (3.10) and (3.16), the pressure shape functions in the water and the interface elevations are written as

$$\{\hat{p}_s^{(1)},\ \hat{p}_s^{(2)}\} = \mathrm{i}\alpha_s\{c,\ \mathrm{i}\tilde{B}_s'/(\alpha_s\tilde{B}_s)\}\cosh[\gamma_s(z+H)]/\cosh(\gamma_s H), \tag{3.23}$$

$$\{\hat{h}_s^{(1)},\ \hat{h}_s^{(2)}\} = \mathrm{i}\gamma_s\{c,\ -\mathrm{i}\tilde{B}_s'/(\alpha_s\tilde{B}_s)\}\tanh(\gamma_s H)/(\alpha_s c^2). \tag{3.24}$$

The pressure fluctuation at the interface can be obtained from (3.1) and (3.23) with $z = 0$. It shows that the peak of pressure fluctuation at the interface occurs behind the wave crest if the wave is growing, or $\mathrm{Re}(\tilde{B}_s'/\tilde{B}_s) > 0$, where Re denotes the real part of a complex variable.

The shape function in the air Φ_s is determined by solving (3.12) with $\hat{c}_s$ replaced by c. This leading-order Rayleigh equation becomes singular at the critical level, z_c, where the wave speed c is equal to the mean velocity $U_c \equiv U(z = z_c)$. In order to account for the nonlinear jump of the streamwise fluctuation velocity across the critical layer, the shape function is expressed as

$$\Phi_s(z, t_1) = \Phi_s^{(a)}(z) + D_s(t_1)\Phi_s^{(b)}(z), \tag{3.25}$$

where $D_s(t_1)$ will be determined from the critical-layer solutions, as in (5.9). In this analysis, both linear and nonlinear effects appear at the same leading order (as in Reutov 1980; Alexakis *et al.* 2004*b*; Lee & Wundrow 2011) in contrast to the Rayleigh instability waves in boundary layers and free shear flows.

By substituting (3.25) into (3.12) and (3.19) with (3.20), one can show that

$$(U - c)(\partial_z^2 - \gamma_s^2)\Phi_s^{(a,b)} - U''\Phi_s^{(a,b)} = 0, \tag{3.26}$$

subject to

$$\Phi_s^{(a)} = (\mathrm{i}/\gamma_s)\partial_z\hat{\phi}_s^{(1)} = \mathrm{i}\tanh(\gamma_s H) \quad \text{at } z = 0, \quad \Phi_s^{(a)} \to 0 \quad \text{as } z \to \infty, \tag{3.27}$$

$$\Phi_s^{(b)} = 0 \quad \text{at } z = 0, \quad \Phi_s^{(b)} \to 0 \quad \text{as } z \to \infty. \tag{3.28}$$

The series expansion of the linear shape function $\Phi_s^{(a)}$ about z_c is obtained by using the Frobenius method (Drazin & Reid 2004) as

$$\Phi_s^{(a)} = b_s[1 + (U_c''/U_c')\tilde{z}(\ln|\tilde{z}| + \hat{b}_s^{\pm} - 1)] + \cdots, \tag{3.29}$$

where we have used

$$U(\tilde{z}) = c + U_c'\tilde{z} + \tfrac{1}{2}U_c''\tilde{z}^2 + \cdots, \tag{3.30}$$

$$\tilde{z} \equiv z - z_c, \quad c = U_c \equiv U(z = z_c), \quad U_c' \equiv U_z(z = z_c), \quad U_c'' \equiv U_{zz}(z = z_c), \tag{3.31}$$

and the superscript $\pm$ in $\hat{b}_s^{\pm}$ denotes the values above and below the critical level, respectively. The complex constant b_s can be determined from the numerical solution of (3.26) with (3.27) as

$$b_s = \Phi_s^{(a)}(z = z_c) = \lim_{z \to z_c^{\pm}} \Phi_s^{(a)}(z). \tag{3.32}$$

By matching the outer solution with the critical-layer solution, we can show that the critical-layer jump of the linear solution, $\hat{b}_s^+ - \hat{b}_s^-$, is equal to $\mathrm{i}\pi$ as given in (5.8) (see also Miles 1957; Drazin & Reid 2004, and others).

The second shape function $\Phi_s^{(b)}$ in (3.25) is the second linearly independent solution of Rayleigh's equation obtained by the method of variation of parameters (Reutov 1980; Drazin & Reid 2004)

$$\Phi_s^{(b)} = \begin{Bmatrix} J_s\Phi_s^{(a)}, & z \geqslant z_c \\ \Phi_s^{(a)}\displaystyle\int_0^z (\Phi_s^{(a)})^{-2}\,\mathrm{d}\xi, & z < z_c \end{Bmatrix}$$
$$= J_s\Phi_s^{(a)} - \begin{Bmatrix} 0, & z \geqslant z_c \\ \Phi_s^{(a)}\displaystyle\int_z^{z_c} (\Phi_s^{(a)})^{-2}\,\mathrm{d}\xi, & z < z_c \end{Bmatrix}, \tag{3.33}$$

where

$$J_s \equiv \int_0^{z_c} (\Phi_s^{(a)})^{-2}\,\mathrm{d}z. \tag{3.34}$$

The series expansion of $\Phi_s^{(b)}$ about the critical level is obtained by substituting (3.29) into (3.33) as

$$\Phi_s^{(b)} = J_s b_s\left[1 + (U_c''/U_c')\tilde{z}(\ln|\tilde{z}| + \hat{b}_s^{\pm} - 1)\right] + \begin{Bmatrix} 0 \\ \tilde{z}/b_s \end{Bmatrix} + \cdots, \tag{3.35}$$

where the last term in braces becomes 0 if $z > z_c$ and $\tilde{z}/b_s$ if $z < z_c$. One can show from (3.33) with (3.27) that $\Phi_s^{(b)}$ was normalized by

$$\partial_z\Phi_s^{(b)} = 1/\Phi_s^{(a)} = -\mathrm{i}/\tanh(\gamma_s H) \quad \text{at } z = 0. \tag{3.36}$$

Although $\Phi_s^{(b)}$ is fully determined by (3.33), it can be computed by directly solving (3.26) with (3.28) and (3.36). We also find that $J_s b_s = \lim_{z\to z_c^{\pm}} \Phi_s^{(b)}(z) = -\mathrm{i}|J_s b_s|$ and $J_s = -\mathrm{i}U_c'\mathrm{Re}(b_s)/(\pi U_c''\,|b_s|^2\,b_s)$: details will be given in a follow-on paper.

It will be shown below that the secondary-mode growth rate is nonlinear (as already noted). The second shape function $\Phi_s^{(b)}(z)$ is introduced to account for the nonlinear effects. Its shape is different from $\Phi_s^{(a)}(z)$ only below the critical level. As will be shown in §§ B.1 and B.2, $\Phi_p^{(b)} = 0$ for the linear primary mode, and $\Phi_d^{(a)} = 0$ for the purely nonlinear difference mode.

Once $\Phi_s^{(a)}$ is solved (for example, numerically), the second-order dynamic interface condition in (3.17), with (3.25), (3.27), (3.28) and (3.36), determines the modal growth rate as

$$\gamma_s[2\mathrm{i}\tilde{B}_s'/(\alpha_s c\tilde{B}_s) + 1] - (U_0'/c)\tanh(\gamma_s H) + \mathrm{i}\partial_z\Phi_s(z=0) = 0. \tag{3.37}$$

The above equation, especially the derivative term $\partial_z\Phi_s(z=0)$, can be expressed in terms of the critical-layer jump condition if the solvability condition is imposed on (3.26) and (3.27). It is derived by multiplying (3.26) by $\Phi_s^{(a)*}$, where $*$ denotes the complex conjugate, to obtain (Nayfeh 1981)

$$\partial(\Phi_s^{(a)*}\partial_z\Phi_s^{(a)})/\partial z = |\partial_z\Phi_s^{(a)}|^2 + [\gamma_s^2 + U''/(U-c)]\,|\Phi_s^{(a)}|^2. \tag{3.38}$$

Integrating over the transverse domain by using the Cauchy principal-value integral

$$⨍_0^{\infty}\mathrm{d}z = \lim_{\hat{\epsilon}\to 0}\left[\int_0^{z_c-\hat{\epsilon}}\mathrm{d}z + \int_{z_c+\hat{\epsilon}}^{\infty}\mathrm{d}z\right], \tag{3.39}$$

along with (3.29) and (3.37), we obtain

$$\left[2\mathrm{i}\gamma_s\tilde{B}_s'/(\alpha_s c\tilde{B}_s)\right]\tanh(\gamma_s H)+(\hat{b}_s^+-\hat{b}_s^-)\,|b_s|^2\,U_c''/U_c'+D_s=R_s, \tag{3.40}$$

where the real constant R_s is given by

$$\begin{aligned}R_s=&-\!\!\!\!\!\!\int_0^\infty[|\partial_z\Phi_s^{(a)}|^2+\{\gamma_s^2+U''/(U-c)\}\,|\Phi_s^{(a)}|^2]\,\mathrm{d}z\\&-\gamma_s\tanh(\gamma_s H)+(U_0'/c)\tanh^2(\gamma_s H).\end{aligned} \tag{3.41}$$

The equation (3.40) will be referred to as the solvability equation. The constants b_s, $\hat{b}_s^\pm$ and R_s are determined from the linear shape function $\Phi_s^{(a)}$, and the function $D_s(t_1)$ is determined by the nonlinear dynamics in the critical layer.

3.5. *Outer solution expansion about critical level*

By substituting (3.25), (B 2) and (B 8) with corresponding (3.29) and (3.35) along with (3.14) into (3.11), and re-expanding the results about the common critical level, we obtain the velocity and pressure field near $z=z_c$ as

$$\begin{aligned}&u-\left(c+U_c'\tilde{z}+\frac{1}{2}U_c''\tilde{z}^2+\cdots\right)\\&\quad=\sum_\iota\epsilon\delta_\iota\tilde{B}_\iota\left[\frac{b_\iota\Omega_\iota}{\cos\theta_\iota}\left\{\frac{\sin^2\theta_\iota}{\tilde{z}}+\frac{U_c''}{U_c'}\left(\ln|\tilde{z}|-\frac{1}{2}\sin^2\theta_\iota+\hat{b}_\iota^\pm\right)\right\}\right.\\&\qquad\left.+\begin{Bmatrix}0\\D_\iota/(b_\iota\cos\theta_\iota)\end{Bmatrix}\right]\mathscr{E}_\iota+\text{c.c.}+\cdots,\end{aligned} \tag{3.42}$$

$$v=-\sum_\iota\epsilon\delta_\iota\tilde{B}_\iota b_\iota\Omega_\iota(\sin\theta_\iota)\left[1/\tilde{z}-\frac{1}{2}(U_c''/U_c')\right]\mathscr{E}_\iota+\text{c.c.}+\cdots, \tag{3.43}$$

$$w=-\sum_\iota\epsilon\delta_\iota\mathrm{i}\gamma_\iota\tilde{B}_\iota b_\iota\Omega_\iota\left[1+(U_c''/U_c')\tilde{z}\left(\ln|\tilde{z}|+\hat{b}_\iota^\pm-1\right)\right]\mathscr{E}_\iota+\text{c.c.}+\cdots, \tag{3.44}$$

$$p-P_0+Gz=\sum_\iota\epsilon\delta_\iota\tilde{B}_\iota b_\iota\Omega_\iota(\cos\theta_\iota)U_c'\mathscr{E}_\iota+\text{c.c.}+\cdots, \tag{3.45}$$

where $\sum_\iota$ denotes the summation of all three modes, i.e. $\sum_\iota(\,)_\iota\equiv(\,)_p+(\,)_s+(\,)_d$, and

$$\delta_p=1,\quad \delta_s=\delta_d=\delta,\quad \Omega_p=1,\quad \Omega_s=1+J_sD_s,\quad \Omega_d=J_dD_d. \tag{3.46}$$

The above equations clearly become singular at the critical level. Therefore, the solution has to be rescaled in this region.

The streamwise velocity jump across the critical layer from the outer solution becomes

$$[u]_{\tilde{z}=-\infty}^{\tilde{z}=+\infty}=\sum_\iota\epsilon\delta_\iota\tilde{B}_\iota(\sec\theta_\iota)\left[(U_c''/U_c')b_\iota\Omega_\iota(\hat{b}_\iota^+-\hat{b}_\iota^-)-D_\iota/b_\iota\right]\mathscr{E}_\iota+\text{c.c.}+\cdots, \tag{3.47}$$

which will be matched with the jump from the critical-layer solution to derive amplitude equations.

4. Critical-layer equations

The thickness of a non-equilibrium critical layer, where the growth effect is balanced with the linear convection effect, must be of the same order as the small

growth rate as in Reutov (1980), Goldstein *et al.* (1987), Goldstein & Choi (1989), Lee & Wundrow (2011) and others. The appropriate vertical coordinate in this region is given as

$$\tilde{\zeta} = (z - z_c)/\sigma = \tilde{z}/\sigma. \tag{4.1}$$

The viscous effect will enter the critical-layer momentum equation while making only relatively insignificant modification in the outer flow when the Reynolds number in air is scaled by

$$1/R_a = \sigma^3 \tilde{\lambda}, \tag{4.2}$$

where the viscous parameter $\tilde{\lambda}$ is order one.

The continuity and momentum equations for the total velocity $\boldsymbol{u} = \boldsymbol{i}u + \boldsymbol{j}v + \boldsymbol{k}w$ and pressure p expressed in terms of the scaled variables t_1, X and $\tilde{\zeta}$ become

$$u_X + v_y + w_{\tilde{\zeta}}/\sigma = 0, \tag{4.3}$$

$$\left[\sigma\frac{\partial}{\partial t_1} + (u-c)\frac{\partial}{\partial X} + v\frac{\partial}{\partial y} + \frac{w}{\sigma}\frac{\partial}{\partial \tilde{\zeta}} - \sigma\tilde{\lambda}\frac{\partial^2}{\partial \tilde{\zeta}^2}\right]\{u, v, w\} = -\left\{p_X, p_y, G + \frac{1}{\sigma}p_{\tilde{\zeta}}\right\}. \tag{4.4}$$

The nonlinear growth effect will balance the linear one in the critical-layer equation of the secondary mode when

$$\epsilon = \sigma^3, \tag{4.5}$$

where ϵ is a measure of the primary-mode steepness as in (2.7), (3.1) and (3.11). Meanwhile, the nonlinear effect due to the coupling of the secondary and difference modes becomes negligibly small when δ, which is a measure of the amplitude ratio of the secondary to primary modes, satisfies

$$\delta \ll 1. \tag{4.6}$$

The nonlinear interaction will generate more than one difference mode when δ becomes $O(1)$, for example, in a subsequent nonlinear-interaction stage as will be shown in a follow-on study.

Introducing (4.1) and (4.5) into the outer solutions (3.42)–(3.45) and re-expanding the result for σ show that the critical-layer solution should be of the form

$$\begin{pmatrix} u \\ v \\ w \\ p \end{pmatrix} = \begin{pmatrix} c + \sigma U_c' \tilde{\zeta} \\ 0 \\ 0 \\ P_0 - Gz \end{pmatrix} + \sigma^2 \begin{pmatrix} u^{(1)} \\ v^{(1)} \\ \sigma w^{(1)} \\ \sigma p^{(1)} \end{pmatrix} + \sigma^3 \ln\sigma \begin{pmatrix} u^{(2L)} \\ v^{(2L)} \\ \sigma w^{(2L)} \\ \sigma p^{(2L)} \end{pmatrix} + \sigma^3 \begin{pmatrix} u^{(2)} \\ v^{(2)} \\ \sigma w^{(2)} \\ \sigma p^{(2)} \end{pmatrix} + \cdots. \tag{4.7}$$

Substituting (4.7) into (4.3) and (4.4) and equating like powers of σ, we obtain

$$Lu^{(\ell)} = -p_X^{(\ell)} - U_c' w^{(\ell)}, \quad Lv^{(\ell)} = -p_y^{(\ell)}, \quad \text{for } \ell = \{1, 2L\}, \tag{4.8}$$

$$Lu^{(2)} = -p_X^{(2)} - U_c' w^{(2)} - u^{(1)} u_X^{(1)} - v^{(1)} u_y^{(1)} - w^{(1)} u_{\tilde{\zeta}}^{(1)}, \tag{4.9}$$

$$Lv^{(2)} = -p_y^{(2)} - u^{(1)} v_X^{(1)} - v^{(1)} v_y^{(1)} - w^{(1)} v_{\tilde{\zeta}}^{(1)}, \tag{4.10}$$

$$u_X^{(\ell)} + v_y^{(\ell)} + w_{\tilde{\zeta}}^{(\ell)} = 0, \quad p_{\tilde{\zeta}}^{(\ell)} = 0 \quad \text{for } \ell = \{1, 2L, 2\}, \tag{4.11}$$

where we have put

$$L \equiv \partial/\partial t_1 + U_c' \tilde{\zeta}\, \partial/\partial X - \tilde{\lambda}\, \partial^2/\partial \tilde{\zeta}^2. \tag{4.12}$$

We must now solve these equations subject to the transverse boundary conditions that they match onto the outer solutions. It is convenient to introduce the critical-layer amplitude $\tilde{A}_\iota$,

$$\tilde{A}_\iota = b_\iota \Omega_\iota \tilde{B}_\iota \quad \text{for } \iota = \{p, s, d\}, \tag{4.13}$$

where $\tilde{B}_\iota$ is the amplitude in the outer solutions given in § 3, and Ω_ι is defined by (3.46). Then, $w^{(1)}$ and $p^{(1)}$ that match onto the outer solutions (3.44) and (3.45) become

$$\begin{pmatrix} w^{(1)} \\ p^{(1)} \end{pmatrix} = \begin{pmatrix} -\mathrm{i}\gamma_p \\ U_c' \cos\theta_p \end{pmatrix} \tilde{A}_p \mathscr{E}_p + \delta \begin{pmatrix} -\mathrm{i}\gamma_s \\ U_c' \cos\theta_s \end{pmatrix} \tilde{A}_s \mathscr{E}_s + \delta \begin{pmatrix} -\mathrm{i}\gamma_d \\ U_c' \cos\theta_d \end{pmatrix} \tilde{A}_d \mathscr{E}_d + \text{c.c.}, \tag{4.14}$$

where $\mathscr{E}_\iota$ is defined in (3.2), and $u^{(1)}$ and $v^{(1)}$ can be written as

$$\begin{aligned} \begin{pmatrix} u^{(1)} - \dfrac{1}{2} U_c'' \tilde{\zeta}^2 \\ v^{(1)} \end{pmatrix} = {} & \mathrm{i} \begin{pmatrix} \tan\theta_p \\ -1 \end{pmatrix} \tilde{Q}_p^{(1)} \mathscr{E}_p + \delta \mathrm{i} \begin{pmatrix} \tan\theta_s \\ -1 \end{pmatrix} \tilde{Q}_s^{(1)} \mathscr{E}_s \\ & + \delta \mathrm{i} \begin{pmatrix} \tan\theta_d \\ -1 \end{pmatrix} \tilde{Q}_d^{(1)} \mathscr{E}_d + \text{c.c.} \end{aligned} \tag{4.15}$$

The second-order critical-layer solution must include all harmonics generated by the nonlinear terms in (4.9) and (4.10). They become, up to $O(\delta)$,

$$\begin{aligned} q^{(2)} = {} & \tilde{Q}_p^{(2)} \mathscr{E}_p + \tilde{Q}_0^{(2)} + \tilde{Q}_{2p}^{(2)} \mathscr{E}_p^2 \\ & + \delta \left[\tilde{Q}_s^{(2)} \mathscr{E}_s + \tilde{Q}_d^{(2)} \mathscr{E}_d + \tilde{Q}_{p+s}^{(2)} \mathscr{E}_p \mathscr{E}_s + \tilde{Q}_{p+d}^{(2)} \mathscr{E}_p \mathscr{E}_d \right] + \text{c.c.}, \end{aligned} \tag{4.16}$$

where $q^{(2)}$ and $\tilde{Q}_J^{(2)}$ denote

$$q^{(2)} \equiv \left\{ u^{(2)} - \tfrac{1}{6} U_c''' \tilde{\zeta}^3,\ v^{(2)},\ w^{(2)},\ p^{(2)} \right\}, \tag{4.17}$$

$$\tilde{Q}_J^{(2)} \equiv \left\{ \tilde{U}_J^{(2)},\ \tilde{V}_J^{(2)},\ \tilde{W}_J^{(2)},\ \tilde{P}_J^{(2)} \right\} \quad \text{for } J = \{p,\ s,\ d,\ 0,\ 2p,\ p+s,\ p+d\}. \tag{4.18}$$

It is noted, from (4.14) and (4.11), that the leading-order vertical fluctuation velocity $w^{(1)}$ and pressure components $p^{(1)}$ and $\tilde{P}_J^{(2)}$ are constant across the critical layer.

By substituting (4.14)–(4.18) into (4.8)–(4.12), a system of critical-layer equations is derived for $\tilde{Q}_\iota^{(1)}$ and $\tilde{Q}_J^{(2)}$ as given in appendix C. They can be analytically integrated as in Goldstein & Choi (1989), Goldstein & Lee (1992) and Wu (1992) for the inviscid case and as in Wu *et al.* (1993) and Wu & Stewart (1996) for the viscous case. The system of partial differential equations can also be solved numerically as in Lee (1997).

5. Amplitude equations

5.1. *Matching of critical-layer jumps*

The critical-layer equations in appendix C are analytically solved to obtain the velocity jumps across the critical layer. The normalized variables

$$\hat{\alpha}_\iota = \alpha_\iota/\bar{\alpha}, \quad \hat{\beta}_\iota = \beta_\iota/\bar{\beta}, \quad \hat{\gamma}_\iota = \gamma_\iota/\bar{\beta}, \tag{5.1}$$

$$\bar{t} = \hat{\kappa}(\bar{\alpha}U_c' t_1 - t_o), \quad \zeta = \tilde{\zeta}/\hat{\kappa} - \tilde{\zeta}_o, \quad \bar{X} = X - X_o, \quad \lambda = \tilde{\lambda}/(\bar{\alpha}\hat{\kappa}^3 U_c'), \tag{5.2}$$

$$A_\iota = (\sqrt{M/U_c'}/\hat{\kappa}^3)\tilde{A}_\iota \mathrm{e}^{\mathrm{i}\hat{\alpha}_\iota(X_o+\tilde{\zeta}_o\bar{t})}, \quad U_\jmath^{(2)} = \left(\bar{\alpha}^2 M/\bar{\beta}^2/\hat{\kappa}^3\right)\tilde{U}_\jmath^{(2)}\mathrm{e}^{\mathrm{i}\hat{\alpha}_\jmath(X_o+\tilde{\zeta}_o\bar{t})} \tag{5.3}$$

are introduced, where the normalization parameters $\hat{\kappa}$ and M, and the coordinate origin shifts t_o, $\tilde{\zeta}_o$ and X_o will be chosen subsequently, as in (E 2), (E 3). The $\bar{\alpha}$ and $\bar{\beta}$ will be chosen later when numerical results are presented, as in (6.4).

The velocity jumps become

$$\int_{-\infty}^{\infty} U_{p\,\zeta}^{(2)}\,\mathrm{d}\zeta = \mathrm{i}\pi(\bar{\alpha}^2/\bar{\beta}^2)\sqrt{M/U_c'}\;U_c''(\sec\theta_p)\,A_p(\bar{t}), \tag{5.4}$$

$$\int_{-\infty}^{\infty} U_{s\,\zeta}^{(2)}\,\mathrm{d}\zeta = \mathrm{i}\pi(\bar{\alpha}^2/\bar{\beta}^2)\sqrt{M/U_c'}\;U_c''(\sec\theta_s)\,A_s(\bar{t}) + F_s(\bar{t}|A_p, A_d^*), \tag{5.5}$$

$$\int_{-\infty}^{\infty} U_{d\,\zeta}^{(2)}\,\mathrm{d}\zeta = (\cos\theta_s/\cos\theta_d)[\mathrm{i}\pi(\bar{\alpha}^2/\bar{\beta}^2)\sqrt{M/U_c'}\;U_c''(\sec\theta_s)A_d(\bar{t}) + F_d(\bar{t}|A_p, A_s^*)]. \tag{5.6}$$

It is shown that the nonlinear jump of a mode is produced by a quadratic interaction of the other two modes, i.e. F_s of the secondary mode by A_p and A_d, and F_d for the difference mode by A_p and A_s. The nonlinear jump for the primary mode, F_p, does not appear in (5.4), since

$$F_p(\bar{t}|A_s, A_d) = 0. \tag{5.7}$$

It is zero because α_p is larger than α_s and α_d. We can show that $\int_{-\infty}^{\infty} V_{\jmath\,\zeta}^{(2)}\,\mathrm{d}\zeta = 0$ for $\jmath = \{p, s, d\}$, as in (C 20). It is also found that the other second-order modes in (4.16), for $\jmath = \{0, 2p, p+s, p+d\}$, do not produce a critical-layer jump as in (C 21). Therefore, these modes only exist inside the thin critical layer and become negligibly small in the outer region.

Matching between the critical-layer solutions (4.7) and the outer solutions (3.42)–(3.45) requires that the velocity jumps (5.4)–(5.6) from the critical-layer solutions at $O(\sigma^3\delta_\iota)$ must be equal to the corresponding (3.47) from the outer solution. This arises from the requirement that the changes in the velocity fluctuations across the critical layer calculated from the external solutions are the same, as they are calculated from the internal solutions.

By matching (3.47) with (5.4)–(5.6) using (4.13) and (C 1), we obtain, for $\iota = \{p, s, d\}$,

$$\hat{b}_\iota^+ - \hat{b}_\iota^- = \mathrm{i}\pi, \tag{5.8}$$

$$D_\iota(\bar{t})B_\iota(\bar{t}) = -\left[\bar{\beta}^2 b_\iota(\cos\theta_s)/(\bar{\alpha}^2\sqrt{U_c'M})\right]F_\iota(\bar{t}), \tag{5.9}$$

where the normalized outer amplitude B_ι is related to A_ι by

$$A_\iota = b_\iota\Omega_\iota B_\iota \quad \text{with } B_\iota = (\sqrt{M/U_c'}/\hat{\kappa}^3)\tilde{B}_\iota \mathrm{e}^{\mathrm{i}\hat{\alpha}_\iota(X_o+\tilde{\zeta}_o\bar{t})}. \tag{5.10}$$

The above equation (5.8)–(5.10) with the solvability equation (3.40) completely determine the evolution of amplitudes. Because of (B 7), there is no solvability

equation for the difference mode. They can be combined to drive more explicit amplitude equations that only include the critical-layer amplitudes A_ι, as shown in appendix E. Amplitude equations become further simplified in the inviscid and viscous limits. The results are summarized in the following subsections.

5.2. *Primary mode amplitude*

The primary mode, whose magnitude of $O(\sigma^3)$ is larger than the other modes, remains linear throughout the whole stage independently of the viscous parameter,

$$A_p = \exp(\bar{t}\,). \tag{5.11}$$

Its linear growth rate and initial amplitude $A_p(\bar{t}=0)$ were normalized to be one as shown in § E.1.

5.3. *Finite-viscosity and inviscid amplitude equations*

The $O(1)$-viscosity amplitude equations (E 10) and (E 17) are rewritten as

$$\frac{\mathrm{d}A_s}{\mathrm{d}\bar{t}} = \kappa_s A_s + \varphi_s \left[\chi_s F_s(\bar{t}|A_p, A_d^*) - \frac{\mathrm{d}F_s(\bar{t}|A_p, A_d^*)}{\mathrm{d}\bar{t}}\right], \tag{5.12}$$

$$A_d = -\varphi_d F_d(\bar{t}|A_p, A_s^*), \tag{5.13}$$

where F_s and F_d are given by (D 1) and (D 2), and κ_s, χ_s, φ_s and φ_d are defined in (E 7), (E 8), (E 12) and (E 19).

In the inviscid limit, where $\lambda = 0$, they reduce to

$$\frac{\mathrm{d}A_s}{\mathrm{d}\bar{t}} = \kappa_s A_s(\bar{t}\,) + \hat{\varphi}_{si}\,\mathrm{e}^{2\bar{t}} \int_{-\infty}^{\bar{t}} K_{inv}(\bar{t}|\,\tilde{t})\, A_s(\tilde{t})\,\mathrm{d}\tilde{t}, \tag{5.14}$$

$$A_d = \hat{\varphi}_{di}\,\mathrm{e}^{\bar{t}} \int_{-\infty}^{\bar{t}} \mathrm{e}^{-(1-\nu)\tilde{\tau}}\,\tilde{\tau}^2 A_s^*(\tilde{t})\,\mathrm{d}\tilde{t}, \tag{5.15}$$

where

$$\begin{aligned} K_{inv} = {} & \mathrm{e}^{-(1-\nu)\tilde{\tau}}\left[(1+\nu-\chi_s)(\tilde{\tau}^2 - 3\tilde{\tau}/\nu + 3/\nu^2) + 2\tilde{\tau} - 3/\nu\right] \\ & - \mathrm{e}^{-(1+\nu)\tilde{\tau}}\left[(1-\nu-\chi_s)(\tilde{\tau}^2 + 3\tilde{\tau}/\nu + 3/\nu^2) + 2\tilde{\tau} + 3/\nu\right], \end{aligned} \tag{5.16}$$

$$\tilde{\tau} = \bar{t} - \tilde{t}, \quad \nu \equiv 1 - \alpha_s/\alpha_p > 0, \tag{5.17}$$

$$\hat{\varphi}_{si} = \tfrac{1}{4}\mu_{si}\,\mu_{di}\,\varphi_s\varphi_d^*/\nu^3, \quad \hat{\varphi}_{di} = -\mu_{di}\varphi_d, \tag{5.18}$$

with μ_{si} and μ_{di} in (D 8). It is noted that the inviscid secondary-mode (5.14) does not include A_d.

The evolution of the secondary wave is governed by an integro-differential equation. Meanwhile, that of the nonlinearly generated difference mode is determined by an integral equation because the free-surface-wave dispersion relation is not satisfied. The integrands, or kernel functions, in (D 1), (D 2) and (5.16) for the viscous and inviscid cases become zero at $\tilde{t}_1 = \bar{t}$ and $\tilde{t} = \bar{t}$. Therefore, the nonlinear jump terms are explicitly determined from the previous histories of amplitudes as in Goldstein & Choi (1989) and other non-equilibrium critical-layer analyses.

The scaling of the primary-wave magnitude ϵ was determined by (4.5) to ensure that the first nonlinear effect appeared at the same order as the linear effect in the secondary-wave dynamics. The resulting amplitude equations describe how the nonlinear critical-layer interaction gradually evolves from the coupling of linear small-steepness surface waves. In the initial stage where $A_p = \exp(\bar{t}\,) \ll 1$, or $O(\epsilon A_p)$ is

smaller than $O(\sigma^3)$, the nonlinear term in the secondary-mode amplitude equation becomes negligibly small and it reduces to a linear equation.

The amplitude equations are solved subject to the initial condition

$$A_s \to a_s\, \mathrm{e}^{\kappa_s \bar{t}} \quad \text{as } \bar{t} \to -\infty. \tag{5.19}$$

The amplitudes A_s and A_d can be normalized as in (E 11) so that the initial value a_s does not appear in the initial condition as shown by (E 13). However, in order to visualize the effect of δ specified in (4.6), by which the magnitudes of the secondary and difference modes are smaller than the primary one, A_s and A_d with an arbitrary small value of a_s will be used to present numerical results in § 6.

Since (5.13) determines the difference-mode amplitude at any $\bar{t}$, its initial amplitude cannot be chosen as a free parameter. However, by putting (5.19) into (5.13) and (5.15), we can show that the difference mode also grows exponentially in the initial linear region. Its growth rate is equal to the sum of the primary linear growth rate and the complex conjugate of the secondary one,

$$A_d \to a_s^* a_d\, \mathrm{e}^{\kappa_d \bar{t}}, \quad \kappa_d = 1 + \kappa_s^*, \quad \text{as } \bar{t} \to -\infty, \tag{5.20}$$

where a_d can be determined from (5.26) for the inviscid and viscous cases. In the viscous limit, from (5.21), $a_d = \hat{\varphi}_{dv}$. Thus, a_d is dependent on λ.

Once the mean wind profile $U(z)$ and the values of c, $\alpha_p(=\omega_p/c)$ and $\alpha_s(=\omega_s/c)$ are specified, the parameters appearing in the amplitude equations, κ_s, χ_s, φ_s, φ_d, etc. are determined from the numerical solutions of $\Phi_p^{(a)}$, $\Phi_s^{(a)}$ and $\Phi_d^{(a)}$ by solving (3.26) subject to (3.27). Note that $\Phi_d^{(a)}$ is solved only to evaluate the parameters, and it is not a part of the outer solution as shown by (B 8).

The above amplitude equations are reasonably simple and relatively easy to solve numerically. There also exist series solutions as will be shown later. The solution of a special inviscid case where K_{inv} becomes zero is given in § F.1. Also, in § F.2, it is shown that the difference-mode amplitude becomes trivial for a two-dimensional secondary wave. If the secondary wave is located at $\tilde{P}$ in figure 3, the nonlinearly generated difference mode at $D_{\tilde{p}}$ becomes steady but spanwise periodic. This special case was studied by Lee & Wundrow (2011). When the secondary mode is at P, the nonlinear interaction becomes that of the primary wave interacting with itself, similar to the case analysed by Goldstein & Leib (1989).

5.4. *Viscous-limit solutions*

In the viscous limit, where $\lambda \to \infty$, the solutions of the amplitude equations become

$$A_s = a_s\, \mathrm{e}^{\kappa_s \bar{t}} \left(1 - \hat{\varphi}_{sv} \mathrm{e}^{2\bar{t}}\right)^{-(\kappa_s - \chi_s + 2)/2}, \quad A_d = a_s^* \hat{\varphi}_{dv} \mathrm{e}^{(1+\kappa_s^*)\bar{t}} \left(1 - \hat{\varphi}_{sv}^* \mathrm{e}^{2\bar{t}}\right)^{-(\kappa_s^* - \chi_s^* + 2)/2}, \tag{5.21}$$

where

$$\hat{\varphi}_{sv} = \mu_{sv}\, \mu_{dv}\, \varphi_s \varphi_d^* / \lambda^2, \quad \hat{\varphi}_{dv} = -\mu_{dv} \varphi_d / \lambda, \tag{5.22}$$

with μ_{sv} and μ_{dv} in (D 10) and (D 11). As will be shown in numerical results, the viscous-limit amplitudes become very large near $\bar{t} = -(1/2)\ln(\mathrm{Re}\,\hat{\varphi}_{sv})$, if $\mathrm{Re}\,\hat{\varphi}_{sv} > 0$, $|\mathrm{Im}\,\hat{\varphi}_{sv}|/|\hat{\varphi}_{sv}| \ll 1$ and $\mathrm{Re}(\kappa_s - \chi_s + 2) > 0$, where Im denotes the imaginary part of a complex variable.

5.5. *Analytic solutions of amplitude equations*

Both inviscid and finite-viscosity amplitude equations (5.12)–(5.15) possess the following absolutely convergent series solutions:

$$A_s(\bar{t}) = \sum_{n=0}^{\infty} s_n \, \mathrm{e}^{(2n+\kappa_s)\,\bar{t}}, \quad A_d(\bar{t}) = \sum_{n=0}^{\infty} d_n \, \mathrm{e}^{(2n+\kappa_s^*+1)\,\bar{t}}. \tag{5.23}$$

The recursion relations are obtained as

$$s_0 = a_s, \tag{5.24}$$

$$s_n = 8\hat{\varphi}_{si}\nu^3\{(2n+\kappa_s-\chi_s)/n\}\,(2n+\kappa_s-\nu-1)^{-3} \times (2n+\kappa_s+\nu-1)^{-3}\; g_{n-1}\, s_{n-1} \quad \text{for } n \geqslant 1, \tag{5.25}$$

$$d_n = 2\,\hat{\varphi}_{di}\,(2n+\kappa_s^*-\nu+1)^{-3}\; h_n\, s_n^* \quad \text{for } n \geqslant 0. \tag{5.26}$$

In the inviscid limit, where $\lambda = 0$, g_{n-1} and h_n become

$$g_{n-1} = h_n = 1 \quad \text{if } \lambda = 0, \tag{5.27}$$

and they are given in appendix G for the finite-viscosity case.

Their asymptotic behaviour when $\bar{t} \to \infty$ is obtained as

$$\left.\begin{aligned} A_s &\sim \hat{a}_s \exp[\tfrac{1}{6}(\kappa_s-\chi_s+1)\bar{t} + 3\,(4\mu_{si}\mu_{di}\varphi_s\varphi_d^*)^{1/6}\,\mathrm{e}^{\bar{t}/3}], \\ A_d &\sim \hat{a}_d A_s^*, \end{aligned}\right\} \tag{5.28}$$

by following Wundrow *et al.* (1994), with $\hat{a}_s$ and $\hat{a}_d$ given in (G 7) and (G 8). It is worth pointing out that there is no undetermined parameter in the above asymptotic forms. The amplitudes A_s and A_d grow like the exponential of an exponential as $\bar{t} \to \infty$ (Goldstein & Lee 1992; Wundrow *et al.* 1994). When $\hat{a}_s = 0$ or $\hat{a}_d = 0$ (see § F.1), (5.28) is invalid, in which case the asymptotic behaviour is determined by higher-order terms.

5.6. *Outer amplitudes B_p and B_s and nonlinear function D_s*

After the critical-layer amplitudes A_s and A_d are solved, the amplitudes B_p and B_s in the outer solutions and the nonlinear function D_s are determined by

$$B_p = \mathrm{e}^{\bar{t}}/b_p, \quad B_s = \left[A_s + \varphi_s F_s(\bar{t}|A_p, A_d^*)\right]/b_s, \quad D_s = [A_s/(b_s B_s) - 1]/J_s, \tag{5.29}$$

where F_s can be evaluated by (D 1), (D 6) or (D 9). The difference mode is solely induced by the nonlinear critical-layer interaction, and B_d always appears multiplied by D_d in the outer solutions (3.42)–(3.45). From (5.10) with (3.46), the $D_d B_d$ becomes

$$D_d B_d = A_d/(b_d J_d). \tag{5.30}$$

The outer solutions in air, (3.11) and (3.42)–(3.45), and the perturbations in water and wave elevation, (2.7), (3.1) and (2.2), are now completely determined.

6. Numerical solutions of amplitude equations

For numerical results presented in this section, a logarithmic profile (Miles 1957, 1993; Morland & Saffman 1993; Janssen 2004) was used for the mean wind,

$$U = 2.5\ln(9.025z + 1), \tag{6.1}$$

and the values of independently controllable parameters were chosen as

$$\sigma = 0.0012, \quad G = 0.05, \quad c = 10, \quad H = 10^{35}. \tag{6.2}$$

For the wind profile (6.1) and the following numerical results, the velocity and length are non-dimensionalized by

$$U_a = u_*, \quad \Delta_a = 9.025 z_o, \tag{6.3}$$

where u_* denotes the friction velocity and z_o is the roughness length. The corresponding Charnock's (1955) constant becomes $\alpha_{CH} \equiv g z_o / u_*^2 = G/9.025 = 5.54 \times 10^{-3}$. The large value of H produces the results in deep water. If we choose u_* to be 0.15 m s^{-1}, as an example, then the dimensional wave speed cu_* becomes 1.5 m s^{-1} and $\Delta_a = 1.2 \times 10^{-4}$ m. The parameter values are chosen to show the characteristic behaviours of the solutions of amplitude equations.

Once the streamwise wavenumbers of the primary and secondary waves α_p and α_s, which satisfy (3.5), are selected, β_p, γ_p, θ_p, β_s, γ_s and θ_s are calculated by (3.7) and (3.22). Those of the difference mode α_d, β_d, γ_d and θ_d are determined from (3.6) and (3.7). The $\bar{\alpha}$ and $\bar{\beta}$ introduced in (5.1) are selected as

$$\bar{\alpha} = \alpha_p, \quad \bar{\beta} = \beta_p, \tag{6.4}$$

by assuming $\beta_p > 0$. The viscous parameter λ defined by (4.2) and (5.2) is considered as a free parameter to investigate its effect on the solutions of amplitude equations. The linear shape functions $\Phi_p^{(a)}$, $\Phi_s^{(a)}$ and $\Phi_d^{(a)}$ are obtained by numerically solving (3.26) subject to (3.27).

The unscaled linear growth rate of the primary mode, as an example, becomes, from (E 4) and (E 16) with (E 2),

$$(\mathrm{d}\tilde{B}_p/\mathrm{d}t)/\tilde{B}_p = \sigma\tilde{\kappa}_p = -\sigma\pi U_c'' c\,|b_p|^2\,\alpha_p(1 - \mathrm{i}\hat{\alpha}_p\,\tilde{\zeta}_o)/[2U_c'\gamma_p \tanh(\gamma_p H)], \tag{6.5}$$

where $|b_p|$ is determined from the neutral Rayleigh solution $\Phi_p^{(a)}$ as in (3.32). The above result was derived for the small density ratio. Meanwhile, the linear growth rates in figure 1 were obtained for an arbitrary density ratio, as $\alpha_p \mathrm{Im}(\hat{c}_p)$ from numerical solutions of (3.12) with complex $\hat{c}_p$ (as in Conte & Miles 1959; Morland & Saffman 1993; Alexakis, Young & Rosner 2002; Janssen 2004, and others). The numerical method used is described in appendix H. It is found that the asymptotic linear growth rates by (6.5) are indistinguishable from those in figure 1 for the entire range of parameters plotted.

The diagram of the $2+1$ mode critical-layer interaction presented in figure 3 is replotted in the (θ, α) coordinates in figure 4(*a*). Since both primary and secondary modes start out as free-surface waves, they are located on the solid curve which depicts the free-surface-wave dispersion relation (3.22) with constant $c = 10$. The corresponding wavenumbers for the primary and secondary waves are plotted in figure 4(*b*). The nonlinear critical-layer interaction between the primary mode P_{30} and any secondary mode on the section $P_{-30} \to S_o \to P_{30}$ will generate a difference mode on the dashed curve $D_{-30} \to D_o \to D_{30}$. Similarly, the primary mode P_{70} and a secondary mode on $P_{-70} \to S_o \to P_{70}$ produces a difference mode on the other dashed curve (on which D_{-20} is located). The wavenumbers α_d, β_d and γ_d and the propagation angle θ_d of difference modes are plotted in figure 5 for these two primary-mode angles, $\theta_p = 30^\circ$ as solid curves and 70° as dotted ones. Since $\alpha_s < \alpha_p$ and $\alpha_d < \alpha_p$, the frequencies of the difference and secondary modes are lower than the primary frequency.

The analytic solutions given in § 5.5 were used to compute the amplitudes. For the results presented in this section, less than 80 terms were summed to obtain convergent values. The numerical procedure developed by Goldstein & Lee (1992) and Lee (1997)

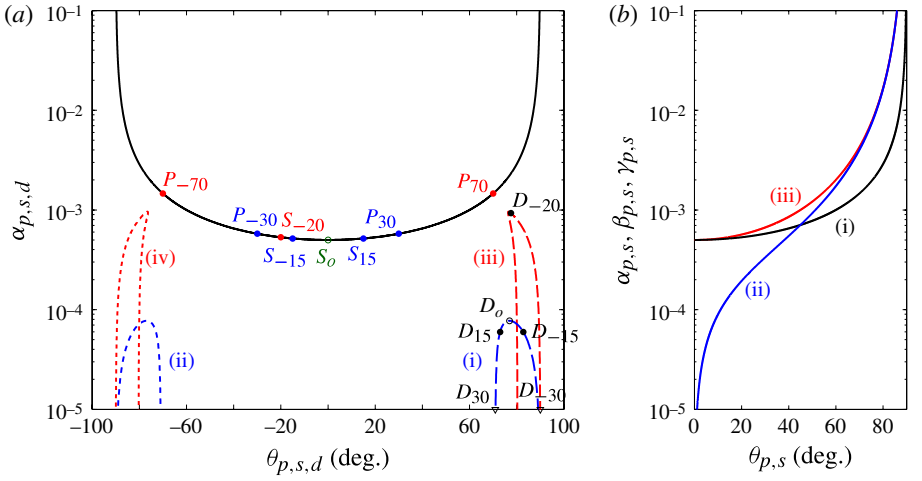

FIGURE 4. (Colour online) (*a*) Diagram of the 2 + 1 mode critical-layer interaction in the (θ, α) coordinates. The primary and secondary modes satisfy the free-surface-wave dispersion relation (black solid curve). The primary mode P_{30} or P_{-30} and a secondary mode on $P_{30} \to S_o \to P_{-30}$ generates a difference mode on the dashed or dotted (blue) curves (i) or (ii). The primary mode P_{70} or P_{-70} and a secondary mode on $P_{70} \to S_o \to P_{-70}$ generate a difference mode on the dashed or dotted (red) curves (iii) or (iv). (*b*) α_p, β_p and γ_p versus θ_p, curves (i)–(iii) respectively, or α_s, β_s and γ_s versus θ_s, curves (i)–(iii) (black, blue and red), respectively.

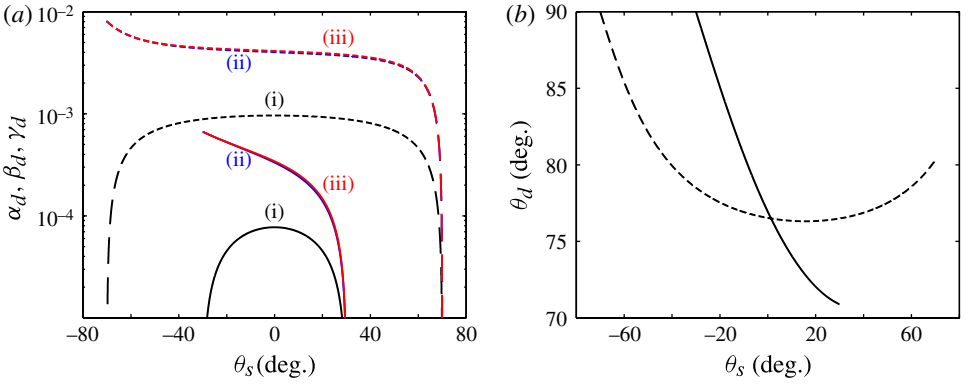

FIGURE 5. (Colour online) (*a*) α_d, β_d and γ_d versus θ_s, curves (i)–(iii) (black, blue and red), respectively, where curves (ii) and (iii) are almost identical, and (*b*) θ_d versus θ_s, when $\theta_p = 30°$ (solid curve) and 70° (dashed curve).

was also used to solve the system of integro-differential amplitude equations. The amplitudes A_s and A_d, with which the summary of equations in § 5 is expressed, are presented in all figures with an arbitrary choice of a_s to emphasize the small scaling factor δ, as mentioned before:

$$a_s = 0.001. \tag{6.6}$$

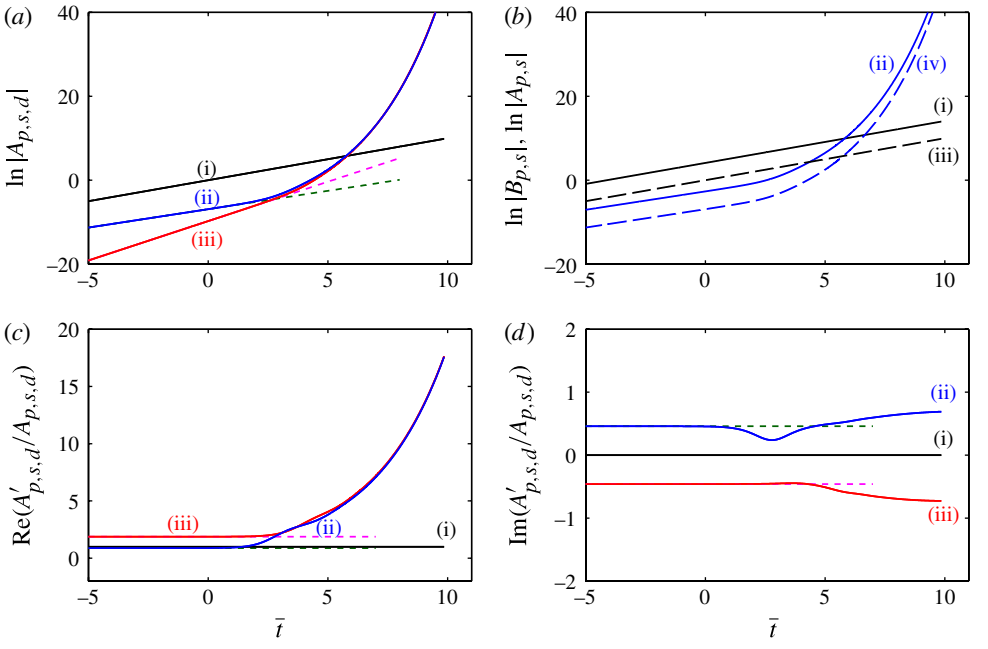

FIGURE 6. (Colour online) Inviscid 2 + 1 mode critical-layer interaction when $\theta_p = 30°$, $\theta_s = -15°$, and $\lambda = 0$. (*a*) $\ln|A_p|$, $\ln|A_s|$ and $\ln|A_d|$, curves (i)–(iii) respectively; (*b*) $\ln|B_p|$, $\ln|B_s|$, $\ln|A_p|$ and $\ln|A_s|$, curves (i)–(iv); (*c*) $\mathrm{Re}(A'_\iota/A_\iota)$ for $\iota = \{p, s, d\}$, curves (i)–(iii); (*d*) $\mathrm{Im}(A'_\iota/A_\iota)$ for $\iota = \{p, s, d\}$, curves (i)–(iii), versus $\bar{t}$. (*a*,*c*,*d*) Solid curves, nonlinear solutions; dotted curves, linear solutions. Primary, secondary and difference modes are in black, blue/green and red/magenta.

Figure 6 illustrates the evolution of amplitudes in the inviscid limit, where $\lambda = 0$. The propagation angles of the primary and secondary waves are chosen to be $\theta_p = 30°$ and $\theta_s = -15°$, as denoted by P_{30} and S_{-15} in figure 4(*a*). For the difference mode, denoted by D_{-15} in the figure, it becomes $\theta_d = 82.8°$. The wave directions in figure 2(*b*) correspond to this case. The wavenumbers are $(\alpha_p, \beta_p, \gamma_p) = (5.8, 3.3, 6.7) \times 10^{-4}$, $(\alpha_s, \beta_s, \gamma_s) = (5.2, -1.4, 5.4) \times 10^{-4}$, and $(\alpha_d, \beta_d, \gamma_d) = (0.6, 4.7, 4.8) \times 10^{-4}$. The primary-mode amplitude A_p grows exponentially throughout the entire stage, as shown in figure 6(*a*). During the linear stage where $\bar{t} < 2$, the secondary-mode amplitude A_s also grows exponentially with the growth rate of κ_s, as well as the difference mode A_d with κ_d, although the latter is nonlinearly generated. Since $\mathrm{Re}(\kappa_d) > \mathrm{Re}(\kappa_s)$ as given by (5.20), A_d becomes as large as A_s near the beginning of the parametric-growth stage. Once the primary amplitude reaches a certain level at $\bar{t} \approx 2$, it starts to affect the growth of the other modes. In the parametric-growth stage where $\bar{t} > 2$, both secondary and difference amplitudes grow much faster than exponential. As shown in figure 6(*a*), A_s and A_d grow almost identically in the later parametric stage where $\bar{t} > 3$. They also grow like the exponential of an exponential as $\bar{t} \to \infty$ (see figure 8 below). The outer amplitude B_p and B_s are shown in figure 6(*b*).

The real parts of A'_ι/A_ι plotted in figure 6(*c*) represent the growth rates. In the exponential-growth stage, they have constant values of 1, 0.88 and 1.88 for the primary, secondary and difference modes, respectively, as shown in the figure

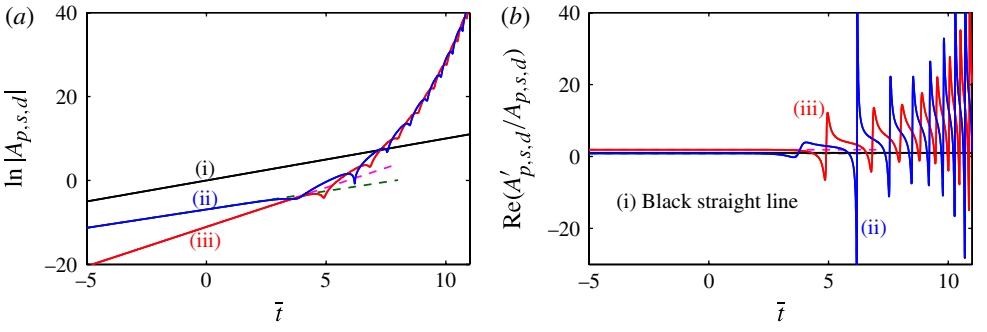

FIGURE 7. (Colour online) Inviscid 2 + 1 mode critical-layer interaction when $\theta_p = 30°$, $\theta_s = 15°$, and $\lambda = 0$. (*a*) $\ln|A_p|$, $\ln|A_s|$ and $\ln|A_d|$, curves (i)–(iii) respectively; (*b*) $\mathrm{Re}(A_\iota'/A_\iota)$ for $\iota = \{p, s, d\}$, curves (i)–(iii), versus $\bar{t}$. Solid curves, nonlinear solutions; dotted curves, linear solutions. Primary, secondary and difference modes are in black, blue/green and red/magenta.

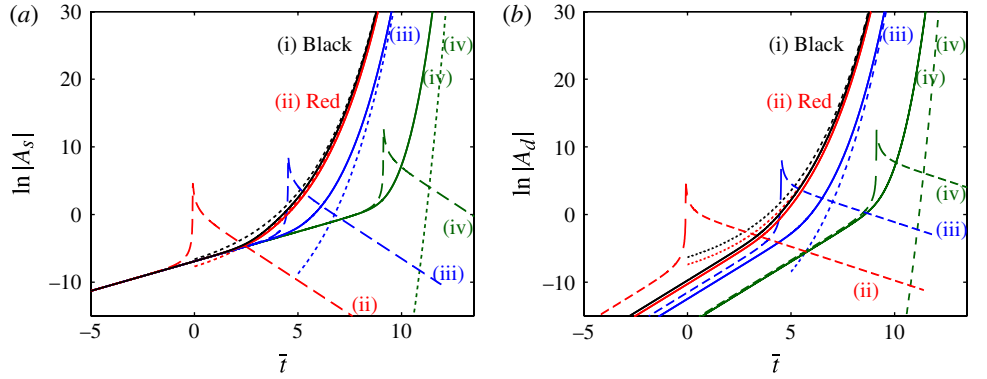

FIGURE 8. (Colour online) Effect of viscosity when $\theta_p = 30°$ and $\theta_s = -15°$. (Black) curve (i), $\lambda = 0$ (inviscid); (red) curve (ii), $\lambda = 10$; (blue) curve (iii), $\lambda = 10^3$; (green) curve (iv), $\lambda = 10^5$. Solid curves, finite-viscosity solutions; dashed curves, viscous-limit solutions; dotted curves, asymptotic solutions. (*a*) $\ln|A_s|$ and (*b*) $\ln|A_d|$ versus $\bar{t}$.

as dotted lines. However, they become very large in the parametric-growth stage as shown by solid curves. The $\mathrm{Re}(A_\iota'/A_\iota)$ also represents the energy transfer rate since $(\mathrm{d}|A_\iota|^2/\mathrm{d}\bar{t})/|A_\iota|^2 = 2\mathrm{Re}(A_\iota'/A_\iota)$. For the entire stage, $\mathrm{Re}(A_s'/A_s - \kappa_s)$ and $\mathrm{Re}(A_d'/A_d - \kappa_d)$ are positive. As a result, the amplitudes grow monotonically. Figure 6(*d*) shows $\mathrm{Im}(A_\iota'/A_\iota)$ which represents the wavelength reduction.

Inviscid results when $\theta_p = 30°$ and $\theta_s = 15°$ with $\lambda = 0$ are shown in figure 7. The θ_d becomes 72.9°, and $(\alpha_d, \beta_d, \gamma_d) = (0.6, 1.9, 2.0) \times 10^{-4}$. As in the previous case given in figure 6, the parametric-growth effects become noticeable near $\bar{t} \approx 2$. The amplitudes become very oscillatory in the parametric-growth stage. In the initial linear stage where A_s and A_d grow exponentially, the signs of $\mathrm{Re}(A_s'/A_s - \kappa_s)$ and $\mathrm{Re}(A_d'/A_d - \kappa_d)$ remain unchanged. Since they are negative in this case, the initial nonlinear effects tend to reduce the growth rates. However, the continuing nonlinear effect enables the reverse of their signs for the eventual exponential-of-an-exponential growth of amplitudes. The sign of $\mathrm{Re}(A_s'/A_s - \kappa_s)$ is first reversed at $\bar{t} \approx 3.7$ followed

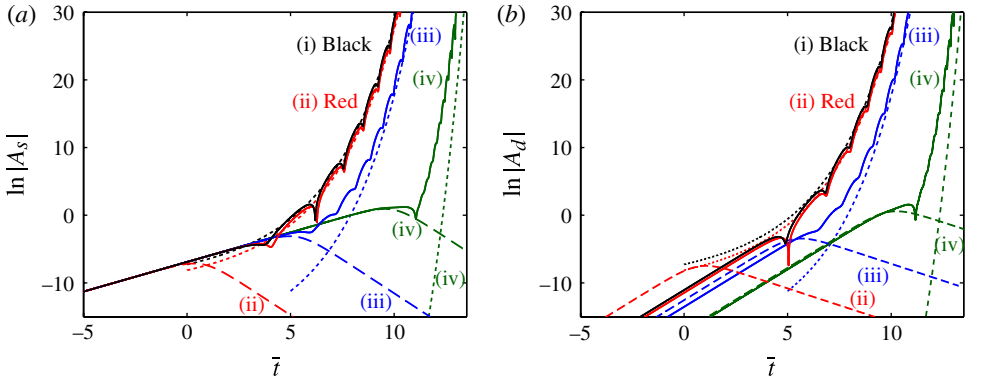

FIGURE 9. (Colour online) Effect of viscosity when $\theta_p = 30°$ and $\theta_s = 15°$. (Black) curve (i), $\lambda = 0$ (inviscid); (red) curve (ii), $\lambda = 10$; (blue) curve (iii), $\lambda = 10^3$; (green) curve (iv), $\lambda = 10^5$. Solid curves, finite-viscosity solutions; dashed curves, viscous-limit solutions; dotted curves, asymptotic solutions. (*a*) $\ln|A_s|$ and (*b*) $\ln|A_d|$ versus $\bar{t}$.

by that of $\mathrm{Re}(A_d'/A_d - \kappa_d)$ at $\bar{t} \approx 4.9$. The amplitude growth is delayed due to the initial adverse nonlinear effect compared to that in figure 6.

The effect of the viscous parameter λ is shown in figure 8 for $\theta_p = 30°$ and $\theta_s = -15°$. The value of λ is varied from 0 (inviscid) to 10^5. The finite-viscosity solutions are plotted as solid curves along with the corresponding viscous-limit solutions as dashed curves. The asymptotic solutions computed by (5.28) are plotted as dotted curves. The finite-viscous solutions when $\lambda = 1$ (not plotted) are almost identical to the inviscid ones. It is shown that the onset of the parametric growth, which can be identified as the departing point from the corresponding linear line (not plotted here, but similar to the dotted lines in figure 6*a*), is delayed as λ is increased. We can also note that A_s and A_d grow almost identically in the later parametric stage. The inviscid and all finite-viscosity solutions approach the exponential-of-an-exponential asymptotic solutions as $\bar{t} \to \infty$. The viscous-limit solutions reach relatively large values before they start to decay. This is due to the near-singular behaviour of the viscous-limit solutions (5.21). The $O(1)$-viscosity solution approaches the viscous-limit solution as λ becomes large, at least at the beginning of the parametric-growth stage. Although they are plotted for different values of λ, in order to compare with the corresponding finite-viscosity solutions, λ is not a freely controllable parameter for the viscous-limit solutions.

Figure 8(*b*) confirms that the initial growth rate of the difference mode in the exponential-growth stage is larger than that of the primary and secondary modes, as expected from (5.20). Its initial amplitude $a_s^* a_d$ is a function of λ (and θ_s). As λ is increased, $a_s^* a_d$ from both finite-viscosity and viscous-limit solutions becomes smaller. The difference between these two becomes smaller with larger λ, and they are almost identical when $\lambda = 10^5$.

Figure 9 shows the effect of λ when $\theta_p = 30°$ and $\theta_s = 15°$. The phenomenon of growth-rate reduction at the beginning of the parametric-growth stage is amplified with larger λ. However, all finite-viscosity solutions become large as $\bar{t} \to \infty$ and approach their asymptotic solutions. The viscous-limit solutions plotted as dashed curves are somewhat different from those in the $\theta_s = -15°$ case shown in figure 8. Without an apparent spike, the amplitudes start to decay at finite $\bar{t}$ because of the negative nonlinear effect.

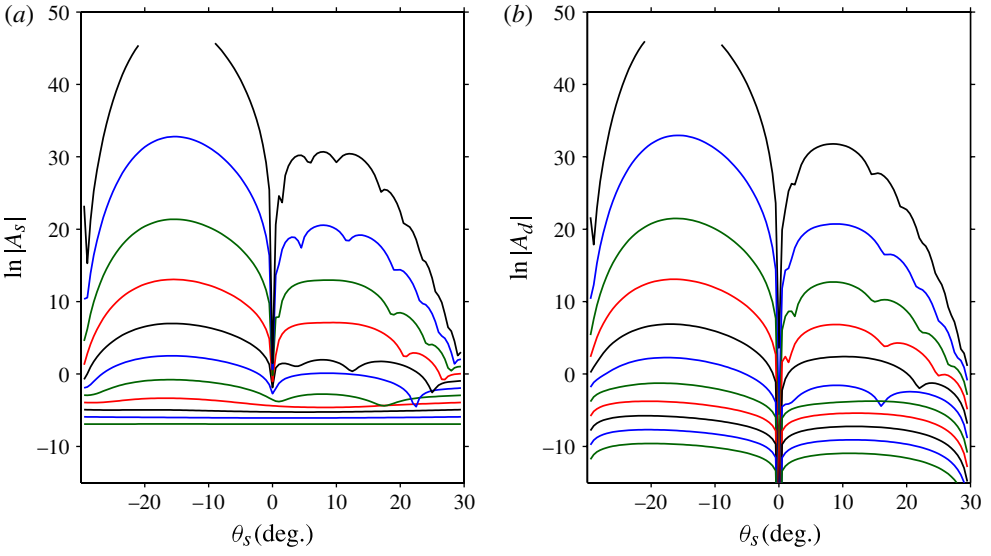

FIGURE 10. (Colour online) Effect of the secondary-wave propagation angle θ_s on inviscid solutions when $\theta_p = 30°$ and $\lambda = 0$. (*a*) $\ln|A_s|$ and (*b*) $\ln|A_d|$ versus θ_s at $\bar{t} = 0, 1, 2, \ldots, 10$, curves from bottom (green) to top (black).

The effect of the secondary-mode propagation angle θ_s on the growth of A_s and A_d was investigated by varying θ_s from -29.5 to $29.5°$ with an increment of $0.5°$, while θ_p was kept constant at $30°$. The inviscid solutions, with $\lambda = 0$, are plotted in figure 10. The inviscid amplitudes grow large as $\bar{t} \to \infty$ for all θ_s, except for a few isolated cases. At $\bar{t} = 9$, shown as the second curve from top, the largest $|A_s|$ occurs when $\theta_s \approx -15°$. For most of θ_s, the nonlinear parametric-growth effect is stronger when the sign of θ_s is opposite to that of θ_p than when both have the same sign.

Figure 10 shows that A_s grows exponentially but A_d becomes zero when the secondary mode is two-dimensional, or $\theta_s = 0°$, as given by (F 2). But a small non-zero value of $|\theta_s|$ can cause large parametric growth effects. The fairly rapid growth of amplitudes when $\theta_s = \pm 0.5°$ shows that the parametric-growth mechanism could still be very effective for the nonlinear growth of nearly two-dimensional surface waves.

Figure 11 shows the effect of θ_s when $\theta_p = 70°$ and $\lambda = 0$. The largest $|A_s|$ occurs when $\theta_s \approx -63°$ at $\bar{t} = 9$ (the second curve from the top). In general, the parametric-growth effect is stronger when the signs of θ_p and θ_s are opposite than when they are equal, as in the previous $\theta_p = 30°$ case. Since $\theta_p > 45°$, the condition in (F 1) is satisfied when $\theta_s = -20°$.

When $\theta_p = 70°$ and $\theta_s = -20°$, they generate a difference mode with $\theta_d = 77.5°$, as denoted by P_{70}, S_{-20} and D_{-20} in figure 4(*a*). The wavenumbers are $(\alpha_p, \beta_p, \gamma_p) = (1.5, 4.0, 4.3) \times 10^{-3}$, $(\alpha_s, \beta_s, \gamma_s) = (5.3, -1.9, 5.7) \times 10^{-4}$, and $(\alpha_d, \beta_d, \gamma_d) = (0.9, 4.2, 4.3) \times 10^{-3}$. This a special inviscid case where (F 1) is satisfied and both secondary and difference modes, as well as the primary one, grow exponentially. The effect of the viscosity in this case is shown in figure 12 with λ varying from 0 to 10^5. When $\lambda = 0$, the inviscid amplitudes grow exponentially, as plotted as straight solid lines. However, a very small viscosity, i.e. $\lambda = 10^{-2}$, destabilizes the linear solution and can cause the large growth of amplitudes. The onset of parametric growth occurs earlier as λ is increased from 0 to 1 (or 10). However, it is delayed when the viscous parameter is further increased.

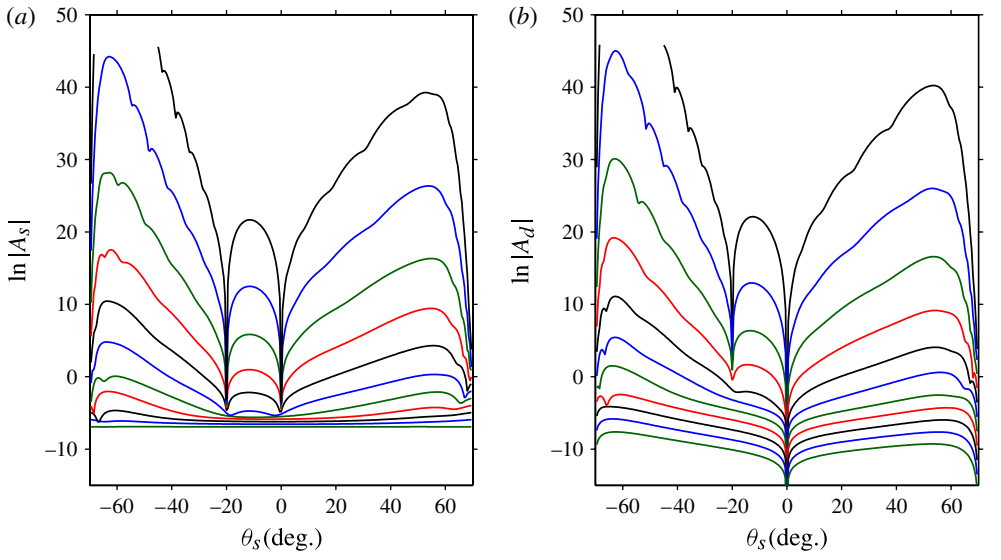

FIGURE 11. (Colour online) Effect of the secondary-wave propagation angle θ_s on inviscid solutions when $\theta_p = 70°$ and $\lambda = 0$. (*a*) $\ln|A_s|$ and (*b*) $\ln|A_d|$ versus θ_s at $\bar{t} = 0, 1, 2, \ldots, 10$, curves from bottom (green) to top (black).

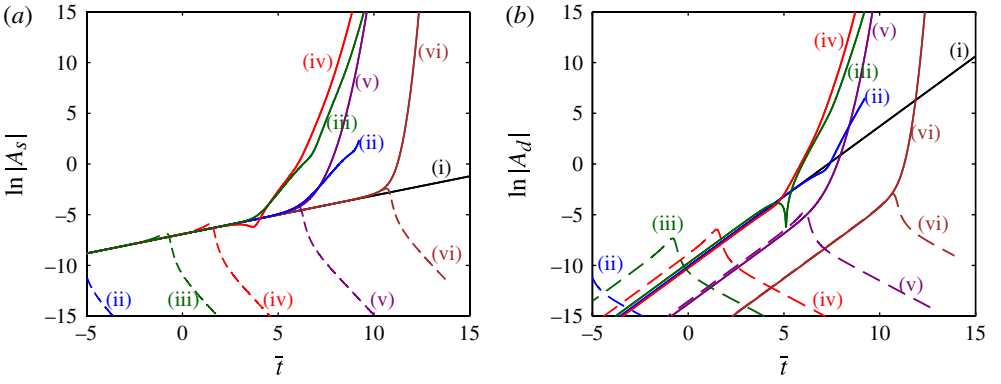

FIGURE 12. (Colour online) Effect of viscosity when $\theta_p = 70°$ and $\theta_s = -20°$. (Black) curve (i), $\lambda = 0$ (inviscid); (blue) curve (ii), $\lambda = 10^{-2}$; (green) curve (iii), $\lambda = 1$; (red) curve (iv), $\lambda = 10$; (purple) curve (v), $\lambda = 10^3$; (brown) curve (vi), $\lambda = 10^5$. Solid curves, finite-viscosity solutions; dashed curves, viscous-limit solutions. (*a*) $\ln|A_s|$ and (*b*) $\ln|A_d|$ versus $\bar{t}$.

7. Discussion

When the wave steepness is small in an initial stage of wave evolution, surface waves grow exponentially due to energy transfer from wind (Miles 1957). The linear growth rates are of $O(\sigma)$ as given by (6.5), where σ is the density ratio of air to water as defined in (2.1). The two-dimensional result in Miles (1957) can be recovered from (6.5) as a special case of zero propagation angle. The waves that travel along the wind direction and that propagate obliquely to wind direction are referred to as two-

dimensional and three-dimensional waves, respectively. Despite continued refinement, the growth rates (of two-dimensional waves) predicted by linear theory are lower by roughly a factor of two than the measurements as summarized in Komen *et al.* (1994), Miles (1997), Janssen (2004), Cavaleri (2007), Sullivan & McWilliams (2010), and others.

A nonlinear interaction occurs when the steepness of surface waves becomes sufficiently large. It can first occur in the critical layer between wave-synchronized air fluctuations, due to the leading-order singularity of Rayleigh's instability equation. The nonlinear critical-layer interaction, then, can affect the growth of surface waves through the air–water interface coupling. If a two-dimensional wave is dominant in an initial wave field, it will go through a nonlinear interaction of a type considered by Reutov (1980) when its steepness becomes $O(\sigma^2)$. However, this strongly nonlinear critical-layer interaction, which only involves two-dimensional modes, reduces its growth rate. Since this happens at very small amplitude, this interaction alone cannot provide a mechanism for a two-dimensional wave to grow as a relevant ocean wave, as mentioned in Reutov (1980).

However, the nonlinear analyses of instability waves in boundary layers and shear flows (Goldstein & Choi 1989; Goldstein & Lee 1992; Wu & Stewart 1996, and others) show that their growth rates can be greatly enhanced when three-dimensional instability waves are involved in a nonlinear interaction process. If their wave speeds are equal, the instability waves share the same critical layer and they can nonlinearly interact there. Because the critical layer is very thin, the pressure and leading-order vertical velocity fluctuations become constant across the layer. The nonlinear governing equations in the critical layer can be analytically solved. By matching these with the solutions outside the critical layer that are still governed by linear equations, one can derive integro-differential or integral equations that describe the evolution of wave amplitudes. This simple principle was implemented in this study to investigate the nonlinear critical-layer effect on the growth of oblique surface waves. The final amplitude equations cover both linear and nonlinear stages, and they describe how the nonlinear critical-layer effects are gradually evolved from the interaction of linear waves. The nonlinear effects become negligibly small in the initial state where the wave steepness is small, and the present amplitude equations reduce to the linear ones of Miles (1957).

A nonlinear critical-layer interaction of obliquely propagating surface waves was studied by using a matched asymptotic analysis. The mean wind is assumed to be two-dimensional. Its profile only depends on the vertical coordinate. The characteristic wave speed is assumed to be sufficiently large, so that the curvature of wind profile is $O(1)$ in the critical layer. Equation (3.8) shows that, for oblique waves with the same wave speed in the wind direction c, the phase speed in the wave direction $\bar{c}_t$ becomes lower and the wavelength becomes shorter as the wave propagation angle θ_t is increased. If the phase speed is equal, the critical-layer location moves away from the interface, or from the viscous sublayer, for an oblique wave with larger propagation angle.

A primary oblique surface wave, that is the largest three-dimensional one, can interact with a secondary (or any other) oblique surface wave of the same wave speed once the primary-mode steepness becomes $O(\sigma^3)$. The secondary-wave elevation can be smaller than that. Note that a two-dimensional wave whose steepness is larger than the primary oblique one can exist. The nonlinear critical-layer interaction between the primary and secondary fluctuations in air, which are synchronized with the corresponding surface waves, generates a difference mode whose frequency and

wavenumbers are equal to the differences between the primary and secondary values. The amplitude of the difference mode is of the order of the secondary-mode amplitude in air where it is generated. In addition, the nonlinear coupling in the critical layer between the primary and difference modes produces a nonlinear growth effect on the secondary wave, when the frequency of the primary wave is larger than the secondary-wave frequency. This nonlinear growth is of the parametric-growth type by which the nonlinear interaction between the primary and difference (or secondary) modes induces a nonlinear growth of the secondary (or difference) mode. Although it plays a critical role in the nonlinear interaction, the primary wave remains as an exponentially growing liner mode during this $2+1$ mode critical-layer interaction stage between two oblique waves and one nonlinearly generated mode. The results in § 5 show that the evolution of the secondary-mode amplitude is governed by an integro-differential equation and that of the difference-mode is determined by an integral equation. Numerical solutions of these equations in the inviscid and finite-viscosity cases, presented in § 6, show that the growth rates of the secondary and difference modes become much larger than the linear growth rates (of the primary and secondary modes) due to the parametric-growth mechanism, except in a few isolated special cases given in appendix F. The analytic solutions in § 5.5 show that the secondary and difference mode amplitudes grow like the exponential of an exponential as $\bar{t} \to \infty$.

Since the difference mode does not satisfy the free-surface-wave dispersion relation (see appendix A), its amplitude in water becomes $O(\sigma)$ smaller than the secondary-wave amplitude. Thus, the wave elevations in water keep their initial order of the largest primary wave, smaller (but rapidly growing) secondary wave, and smallest (rapidly growing) difference mode. However, in air where the actual nonlinear interaction takes place, both secondary and difference mode amplitudes are of the same order of magnitude. The numerical results in figures 6(*a*) and 7(*a*) show that their amplitudes in air indeed grow almost identically in the later stage of the $2+1$ mode interaction. This indicates that the multi-mode generation process in air starts earlier than in water.

The present analysis shows that the first nonlinear interaction between free-surface waves can occur in air, not in water. The nonlinear coupling between surface-wave-induced fluctuations occurs within the critical layer, while the perturbed flows outside the thin critical layer are governed by linear equations. The nonlinear critical-layer interaction affects the growth of the surface-wave-induced fluctuations in air, and then induces the nonlinear growth of surface waves. The mode–mode coupling in the critical layer also generates nonlinear modes (e.g. difference mode) which can induce corresponding fluctuations in air and nonlinear waves in water. It is worth noticing that the present analysis and Lee & Wundrow (2011) are the first to show that the nonlinear growth, which is much faster than the exponential growth, of a free-surface wave can be governed by a nonlinear mode–mode interaction that occurs in the air.

The rapid parametric-growth rate can become explosively large in a later nonlinear stage. By considering a pair of oblique free-surface waves of the same streamwise but opposite spanwise wavenumbers, whose normalized amplitudes are $O(\sigma^{5/2})$, Lee & Wundrow (2011) show that the wave growth is governed by the cubic self-interaction of oblique modes as in Goldstein & Choi (1989). They also show that the cubic interaction generates a large number of spanwise harmonics, whose spanwise wavenumbers are odd multiples of the primary ones of the original pair. As the obliqueness of a higher spanwise mode is increased, its wavelength becomes shorter and its growth will be affected by the viscosity, which will be investigated later. These nonlinearly generated spanwise harmonics are as large as the original pair of oblique

modes in air. The amplitudes of the original pair are governed by fully coupled integro-differential equations, and those of higher spanwise harmonics are determined by integral equations. The inviscid numerical results in Lee & Wundrow (2011) show that all amplitudes grow very fast and eventually become singular at a finite time. This process can be responsible for generating multi-directional oblique modes of the same frequency.

During these nonlinear stages, oblique surface waves play a dominant role. They lead to the parametric-growth interaction in an initial nonlinear stage and they also drive the cubic self-interaction in a later nonlinear stage.

Because of the free-surface-wave dispersion relation (3.22), the streamwise wavenumber of a two-dimensional surface wave is always smaller than the oblique ones as shown in figure 3. This prevents the direct nonlinear coupling between a two-dimensional and an oblique free-surface wave from producing a nonlinear critical-layer jump for a difference mode. By including a two-dimensional surface wave in this analysis, we can show that an exponentially growing two-dimensional wave remains passive if its magnitude is smaller than $O(\sigma^2)$. However, figures 3 and 4(a) indicate that the present $2+1$ mode critical-layer interaction can generate a difference mode whose streamwise wavenumber is smaller than the corresponding two-dimensional one. In this case, the nonlinear coupling between the difference mode and a two-dimensional surface wave of $O(\sigma^2)$ magnitude can affect the growth of the former similar to the Rayleigh instability waves in shear flows shown by Wu & Stewart (1996). The interaction between two-dimensional and oblique modes becomes fully coupled when the oblique modes become sufficiently large. In this fully coupled stage, the oblique modes could be still smaller than the two-dimensional wave, although they are mostly responsible for the explosive growth of all waves including the two-dimensional one (similar to Goldstein & Lee 1992; Wu & Stewart 1996).

Numerical results of the $2+1$ mode interaction given in § 6 show that the parametric-growth effect is stronger when the signs of the propagation angles of the primary and secondary surface waves are opposite than when they are equal. Furthermore, the cubic self-interaction strongly enhances the growth of a pair of oblique surface waves with opposite propagation angles as shown in Lee & Wundrow (2011) even when one of them is initially smaller than the other. These findings could possibly explain the regular rhomboid-like structures that could be recognized in the lower photo on Kinsman (1965, p. 542).

The results from the present analysis and self-interaction study by Lee & Wundrow (2011) show that the nonlinear growth rates of obliquely propagating surface waves can become much larger than the linear growth rates even when their steepnesses are very small. The enhanced nonlinear growth of a secondary surface wave can occur when its steepness is smaller than $O(\sigma^3)$, by interacting with the primary wave of $O(\sigma^3)$ magnitude, according to the present analysis. The explosive growth of Lee & Wundrow (2011) can occur when the wave steepnesses are $O(\sigma^{5/2})$, where a typical value of σ is $O(10^{-3})$. This implies that the purely linear-growth-rate stage may be limited to the case where the wave steepness is very small.

Direct numerical simulations in two dimensions were conducted by Alexakis *et al.* (2004*a*). Since they were interested in astrophysical events, the density ratio of their simulations was 0.1, much larger than in the water-wave case. Their numerical results of two-dimensional wave evolution are in quantitative agreement with the linear theory (Miles 1957; Alexakis *et al.* 2002) and qualitative agreement with the weakly nonlinear theory (Alexakis *et al.* 2004*b*). Although the gravity becomes much larger in the astrophysical environments, the results from the nonlinear critical-layer analysis

by Alexakis *et al.* (2004*b*) are essentially the same as those obtained by Reutov (1980) for a two-dimensional water wave. By resolving the critical-layer dynamics as in Alexakis *et al.* (2004*a*), a direct numerical simulation may be able to capture the present nonlinear interaction. In order to verify the present nonlinear mechanism experimentally, we may have to consider a larger spatial domain or need a wider water tank (e.g. Caulliez & Collard 1999) because it involves multiple three-dimensional waves of different propagation directions.

Acknowledgements

This work was supported by the ONR-funded In-House Laboratory Independent Research (ILIR) program at NSWCCD. The author would like to thank Dr J. Barkyoumb, Dr I. Koh, Mr. T. Applebee and Mr. S. Littlefield for their support. The author is grateful to Dr D. Wundrow for many important suggestions and helpful discussions throughout the course of this work. The outer solution expansions in this paper mostly followed his unpublished manuscript. The author thanks Dr M. E. Goldstein and referees for helpful comments.

Appendix A. Free-surface-wave dispersion relation for the difference mode

For the primary and secondary waves, $(\alpha_p, \beta_p, \gamma_p)$ and $(\alpha_s, \beta_s, \gamma_s)$ satisfy the free-surface-wave dispersion relations (3.22) for a given c.

If $\beta_p\beta_s < 0$, then $|\beta_d| \equiv |\beta_p - \beta_s| > |\beta_p|$. Thus, $\alpha_d (< \alpha_p)$ and β_d, defined by (3.6), do not satisfy the relation (3.22).

For the case when $\beta_p\beta_s > 0$, it is convenient to introduce $\tilde{\beta}_s$ and $\tilde{\beta}_d$,

$$\tilde{\beta}_s = (\beta_p/\alpha_p)\alpha_s, \quad \tilde{\beta}_d = (\beta_p/\alpha_p)\alpha_d, \tag{A 1}$$

then

$$\tilde{\beta}_s^2 - \beta_s^2 = (c^4/G^2)\alpha_s^2[\alpha_p^2/\tanh^2(\gamma_p H) - \alpha_s^2/\tanh^2(\gamma_s H)] = \alpha_s^2(\gamma_p^2/\alpha_p^2 - \gamma_s^2/\alpha_s^2), \tag{A 2}$$

for any pair of (α_s, β_s) that satisfies (3.22). One can also show that $\mathrm{d}(\gamma_s/\alpha_s)/\mathrm{d}\alpha_s \geqslant 0$ from (3.22), and therefore, for $0 < [\alpha_{2D}] < \alpha_s < \alpha_p$,

$$\tilde{\beta}_s^2 - \beta_s^2 > 0 \quad \text{if } \gamma_\iota H > 0, \quad \tilde{\beta}_s^2 - \beta_s^2 \to 0 \quad \text{if } \gamma_\iota H \to 0, \tag{A 3}$$

where $\iota = \{p, s\}$. Because

$$\left.\begin{aligned} &\beta_d^2 \equiv (\beta_p - \beta_s)^2 > (\beta_p - \tilde{\beta}_s)^2 = [(\beta_p/\alpha_p)\alpha_d]^2 \equiv \tilde{\beta}_d^2, \quad \text{or} \\ &\tilde{\beta}_d^2 - \beta_d^2 < 0, \quad \text{if } \gamma_\iota H > 0, \end{aligned}\right\} \tag{A 4}$$

$$\left.\begin{aligned} &\beta_d^2 \equiv (\beta_p - \beta_s)^2 \to (\beta_p - \tilde{\beta}_s)^2 = [(\beta_p/\alpha_p)\alpha_d]^2 \equiv \tilde{\beta}_d^2, \quad \text{or} \\ &\tilde{\beta}_d^2 - \beta_d^2 \to 0, \quad \text{if } \gamma_\iota H \to 0, \end{aligned}\right\} \tag{A 5}$$

the difference mode does not satisfy the free-surface-wave dispersion relation (3.22) when $\gamma_\iota H$ is finite, but that is satisfied in the shallow-water limit where $\tanh(\gamma_\iota H) \to \gamma_\iota H$. However, when $\beta_p\beta_s > 0$ in the shallow-water limit, μ_{s1}, μ_{s2}, μ_{d1} and μ_{d2} in (D 4) and (D 5) become zero. Thus, both secondary and difference modes grow exponentially.

Appendix B. Outer solutions of the primary and difference modes

B.1. *Outer solution of the primary mode*

The critical-layer solutions show that there is no nonlinear velocity jump across the critical layer for the primary mode, as given in (5.4) and (5.7). Thus, from (5.9),

$$D_p = 0. \tag{B 1}$$

The shape function in air is now written without the nonlinear contribution in (3.25):

$$\Phi_p(z) = \Phi_p^{(a)}(z). \tag{B 2}$$

The outer solutions of the linear primary mode become (3.20)–(3.24), (3.26), (3.27), (3.29)–(3.32) and (3.37)–(3.41) with subscript p (instead of s) along with (B 1) and (B 2).

B.2. *Outer solution of the difference mode*

It is assumed that the difference mode is not a free-surface wave, for simplicity (see appendix A). The velocity potentials of the difference mode in water become

$$\hat{\phi}_d^{(1)} = 0, \quad \hat{\phi}_d^{(2)} = \tilde{d}\cosh[\gamma_d(z+H)]D_d(t_1)/\cosh(\gamma_d H), \tag{B 3}$$

where

$$\tilde{d} = \alpha_d c^2(\cos\theta_d)/[\{G\gamma_d\tanh(\gamma_d H) - \alpha_d^2 c^2\}\tanh(\gamma_d H)]. \tag{B 4}$$

The pressure shape functions in water and the interface elevations become

$$\hat{p}_d^{(1)} = 0, \quad \hat{p}_d^{(2)} = \mathrm{i}\,\tilde{d}\,\alpha_d c\, D_d(t_1)\cosh[\gamma_d(z+H)]/\cosh(\gamma_d H), \tag{B 5}$$

$$\hat{h}_d^{(1)} = 0, \quad \hat{h}_d^{(2)} = \mathrm{i}\,\tilde{d}\,(\sec\theta_d)\tanh(\gamma_d H)D_d(t_1)/c. \tag{B 6}$$

Since there is no leading-order velocity potential $\hat{\phi}_d^{(1)}$ in water, the linear shape function $\Phi_d^{(a)}$ in (3.25) that satisfies the interface condition (3.19) must be trivial:

$$\Phi_d^{(a)} = 0. \tag{B 7}$$

Therefore, the shape function in air (3.25) is rewritten as

$$\Phi_d(z, t_1) = D_d(t_1)\Phi_d^{(b)}(z), \tag{B 8}$$

where $\Phi_d^{(b)}$ is still governed by (3.26) subject to (3.28). The difference mode in the outer region is entirely due to the nonlinear interaction in the critical layer.

We note that the leading-order equation (3.26) with (3.27), or $\Phi_d^{(a)} = \mathrm{i}\tanh(\gamma_d H)$ at $z = 0$, and $\Phi_d^{(a)} \to 0$ as $z \to \infty$, still has a solution $\Phi_d^{(a)}$ for a given γ_d and c. With this artificial solution, one can continue to express $\Phi_d^{(b)}$ by (3.33). The outer solution of the difference mode is given by (3.26)–(3.36), with subscript d, and (B 3)–(B 8).

The dynamic interface condition (3.17) was used to derive the solutions (B 3), instead of obtaining the growth-rate relation (3.37). There is no solvability equation for the difference mode. The second shape function, $\Phi_d^{(b)}$, is normalized by $\partial_z\Phi_d^{(b)}(z=0) = -\mathrm{i}/\tanh(\gamma_d H)$ following (3.36), or equivalently by (3.27) through the fictitious solution $\Phi_d^{(a)}$.

As shown in appendix A, the difference mode can satisfy the free-surface-wave dispersion relation in the shallow water limit, where $\tanh(\gamma_t H) \to \gamma_t H$, if the signs of the propagation angles of the primary and secondary waves are equal. In this case, $\hat{\phi}_d^{(1)}$

is not zero and the outer solution of the difference mode must include the linear effect similar to the secondary-mode solution.

Appendix C. System of critical-layer equations

The normalized variables in (5.1) and (5.2), with

$$\{A_\iota, Q_\iota\} = \{\tilde{A}_\iota/\hat{\kappa}, \tilde{Q}_\iota^{(1)}/\sin\theta_\iota\}(\sqrt{M/U_c'}/\hat{\kappa}^2)\mathrm{e}^{\mathrm{i}\hat{\alpha}_\iota(X_o+\tilde{\zeta}_o\bar{t})}, \tag{C 1}$$

are used for the critical-layer equations. The variables represented by $\tilde{Q}_J^{(2)}$ in (4.18) are also normalized as

$$\{U_J^{(2)}, V_J^{(2)}, W_J^{(2)}, P_J^{(2)}\} = \left\{\frac{\bar{\alpha}}{\bar{\beta}}\tilde{U}_J^{(2)},\ \tilde{V}_J^{(2)},\ \frac{\mathrm{i}}{\bar{\beta}\hat{\kappa}}\tilde{W}_J^{(2)},\ \frac{\bar{\beta}}{\bar{\alpha}\hat{\kappa}U_c'}\tilde{P}_J^{(2)}\right\}\frac{\bar{\alpha}M}{\bar{\beta}\hat{\kappa}^3}\,\mathrm{e}^{\mathrm{i}\hat{\alpha}_J(X_o+\tilde{\zeta}_o\bar{t})}, \tag{C 2}$$

with $\hat{\alpha}_J$ given below by (C 6).

The system of normalized equations, which we refer to as the critical-layer equations, now becomes at leading order, for $\iota = \{p, s, d\}$,

$$\mathscr{L}_\iota Q_\iota = \hat{\alpha}_\iota A_\iota, \tag{C 3}$$

subject to the transverse boundary condition, $Q_\iota \propto 1/\zeta \quad \text{as } \zeta \to \infty$, where we have put

$$\mathscr{L}_\iota \equiv \frac{\partial}{\partial\bar{t}} + \mathrm{i}\hat{\alpha}_\iota\zeta - \lambda\frac{\partial^2}{\partial\zeta^2}. \tag{C 4}$$

The second-order critical-layer equations can be written as

$$\mathscr{L}_J\{V_J^{(2)},\ W_{J\,\zeta\zeta}^{(2)},\ U_{J\,\zeta}^{(2)}\} = \{R_{vJ}^{(2)},\ R_{wJ}^{(2)},\ R_{uJ}^{(2)}\}, \quad W_{J\,\zeta}^{(2)} = \hat{\alpha}_J U_J^{(2)} + \hat{\beta}_J V_J^{(2)}, \quad P_{J\,\zeta}^{(2)} = 0, \tag{C 5}$$

for $J = \{p, s, d, 0, 2p, p+s, p+d\}$, where

$$\hat{\alpha}_0 = 0, \quad \hat{\alpha}_{2p} = 2\hat{\alpha}_p, \quad \hat{\alpha}_{p+s} = \hat{\alpha}_p + \hat{\alpha}_s, \quad \hat{\alpha}_{p+d} = \hat{\alpha}_p + \hat{\alpha}_d = 2\hat{\alpha}_p - \hat{\alpha}_s, \tag{C 6}$$

$$\hat{\beta}_0 = 0, \quad \hat{\beta}_{2p} = 2\hat{\beta}_p, \quad \hat{\beta}_{p+s} = \hat{\beta}_p + \hat{\beta}_s, \quad \hat{\beta}_{p+d} = \hat{\beta}_p + \hat{\beta}_d = 2\hat{\beta}_p - \hat{\beta}_s. \tag{C 7}$$

The first equation in (C 5) becomes

$$\mathscr{L}_p V_p^{(2)} = -\mathrm{i}\hat{\beta}_p P_p^{(2)} - \tfrac{1}{2}(\bar{\alpha}/\bar{\beta})\sqrt{M/U_c'}\ U_c''\,\hat{\alpha}_p(\sin\theta_p)\,(\zeta+\tilde{\zeta}_o)^2\,Q_p, \tag{C 8}$$

$$\mathscr{L}_p W_{p\,\zeta\zeta}^{(2)} = \mathrm{i}(\bar{\alpha}/\bar{\beta})\sqrt{M/U_c'}\ U_c''\,\hat{\alpha}_p\hat{\gamma}_p A_p, \tag{C 9}$$

$$\begin{aligned}\mathscr{L}_s V_s^{(2)} = {} & -\mathrm{i}\hat{\beta}_s P_s^{(2)} - \tfrac{1}{2}(\bar{\alpha}/\bar{\beta})\sqrt{M/U_c'}\ U_c''\,\hat{\alpha}_s(\sin\theta_s)\,(\zeta+\tilde{\zeta}_o)^2\,Q_s \\ & - \hat{\gamma}_p(\sin\theta_d)A_p Q_{d\,\zeta}^* - \hat{\gamma}_d(\sin\theta_p)A_d^* Q_{p\,\zeta} \\ & - \mathrm{i}(\hat{\beta}_p/\hat{\alpha}_p - \hat{\beta}_d/\hat{\alpha}_d)\hat{\alpha}_{p+d}(\sin\theta_p\sin\theta_d)Q_p Q_d^*,\end{aligned} \tag{C 10}$$

$$\begin{aligned}\mathscr{L}_s W_{s\,\zeta\zeta}^{(2)} = {} & \mathrm{i}(\bar{\alpha}/\bar{\beta})\sqrt{M/U_c'}\ U_c''\,\hat{\alpha}_s\hat{\gamma}_s A_s - (\hat{\beta}_p/\hat{\alpha}_p - \hat{\beta}_d/\hat{\alpha}_d)[\hat{\alpha}_p\hat{\gamma}_p(\sin\theta_d)A_p Q_{d\,\zeta\zeta}^* + \hat{\alpha}_d\hat{\gamma}_d \\ & \times(\sin\theta_p)A_d^* Q_{p\,\zeta\zeta} + \mathrm{i}2(\hat{\beta}_p/\hat{\alpha}_p - \hat{\beta}_d/\hat{\alpha}_d)\hat{\alpha}_p\hat{\alpha}_d(\sin\theta_p\sin\theta_d)\,(Q_p Q_d^*)_\zeta],\end{aligned} \tag{C 11}$$

$$\begin{aligned}\mathscr{L}_d V_d^{(2)} = {} & -\mathrm{i}\hat{\beta}_d P_d^{(2)} - \tfrac{1}{2}(\bar{\alpha}/\bar{\beta})\sqrt{M/U_c'}\ U_c''\,\hat{\alpha}_d(\sin\theta_d)\,(\zeta+\tilde{\zeta}_o)^2\,Q_d - \hat{\gamma}_p(\sin\theta_s)A_p Q_{s\,\zeta}^* \\ & - \hat{\gamma}_s(\sin\theta_p)A_s^* Q_{p\,\zeta} - \mathrm{i}(\hat{\beta}_p/\hat{\alpha}_p - \hat{\beta}_s/\hat{\alpha}_s)\hat{\alpha}_{p+s}(\sin\theta_p\sin\theta_s)Q_p Q_s^*,\end{aligned} \tag{C 12}$$

$$\begin{aligned}\mathscr{L}_d W_{d\,\zeta\zeta}^{(2)} = {} & \mathrm{i}(\bar{\alpha}/\bar{\beta})\sqrt{M/U_c'}\ U_c''\,\hat{\alpha}_d\hat{\gamma}_d A_d - (\hat{\beta}_p/\hat{\alpha}_p - \hat{\beta}_s/\hat{\alpha}_s)[\hat{\alpha}_p\hat{\gamma}_p(\sin\theta_s)A_p Q_{s\,\zeta\zeta}^* + \hat{\alpha}_s\hat{\gamma}_s \\ & \times(\sin\theta_p)A_s^* Q_{p\,\zeta\zeta} + \mathrm{i}2(\hat{\beta}_p/\hat{\alpha}_p - \hat{\beta}_s/\hat{\alpha}_s)\hat{\alpha}_p\hat{\alpha}_d(\sin\theta_p\sin\theta_s)\,(Q_p Q_s^*)_\zeta],\end{aligned} \tag{C 13}$$

$$\mathscr{L}_0 V_0^{(2)} = -\hat{\beta}_p A_p Q_p^*{}_\zeta, \quad \mathscr{L}_0 U_{0\,\zeta}^{(2)} = (\hat{\beta}_p^2/\hat{\alpha}_p) A_p Q_p^*{}_{\zeta\zeta}, \quad W_{0\,\zeta}^{(2)} = 0, \tag{C 14}$$

$$\mathscr{L}_{2p} V_{2p}^{(2)} = -\mathrm{i}\hat{\beta}_{2p} P_{2p} + \hat{\beta}_p A_p Q_{p\,\zeta}, \quad \mathscr{L}_{2p} W_{2p\,\zeta\zeta}^{(2)} = 0, \tag{C 15}$$

$$\begin{aligned}\mathscr{L}_{p+s} V_{p+s}^{(2)} = {} & -\mathrm{i}\hat{\beta}_{p+s} P_{p+s}^{(2)} + \hat{\gamma}_p(\sin\theta_s) A_p Q_{s\,\zeta} + \hat{\gamma}_s(\sin\theta_p) A_s Q_{p\,\zeta} \\ & + \mathrm{i}(\hat{\beta}_p/\hat{\alpha}_p - \hat{\beta}_s/\hat{\alpha}_s)\hat{\alpha}_d(\sin\theta_p \sin\theta_s) Q_p Q_s,\end{aligned} \tag{C 16}$$

$$\begin{aligned}\mathscr{L}_{p+s} W_{p+s\,\zeta\zeta}^{(2)} = {} & (\hat{\beta}_p/\hat{\alpha}_p - \hat{\beta}_s/\hat{\alpha}_s)[\hat{\alpha}_p\hat{\gamma}_p(\sin\theta_s) A_p Q_{s\,\zeta\zeta} - \hat{\alpha}_s\hat{\gamma}_s(\sin\theta_p) A_s Q_{p\,\zeta\zeta} \\ & - \mathrm{i}2(\hat{\beta}_p/\hat{\alpha}_p - \hat{\beta}_s/\hat{\alpha}_s)\hat{\alpha}_p\hat{\alpha}_s(\sin\theta_p \sin\theta_s)\,(Q_p Q_s)_\zeta],\end{aligned} \tag{C 17}$$

$$\begin{aligned}\mathscr{L}_{p+d} V_{p+d}^{(2)} = {} & -\mathrm{i}\hat{\beta}_{p+d} P_{p+d}^{(2)} + \hat{\gamma}_p(\sin\theta_d) A_p Q_{d\,\zeta} + \hat{\gamma}_d(\sin\theta_p) A_d Q_{p\,\zeta} \\ & + \mathrm{i}(\hat{\beta}_p/\hat{\alpha}_p - \hat{\beta}_d/\hat{\alpha}_d)\hat{\alpha}_s(\sin\theta_p \sin\theta_d) Q_p Q_d,\end{aligned} \tag{C 18}$$

$$\begin{aligned}\mathscr{L}_{p+d} W_{p+d\,\zeta\zeta}^{(2)} = {} & (\hat{\beta}_p/\hat{\alpha}_p - \hat{\beta}_d/\hat{\alpha}_d)[\hat{\alpha}_p\hat{\gamma}_p(\sin\theta_d) A_p Q_{d\,\zeta\zeta} - \hat{\alpha}_d\hat{\gamma}_d(\sin\theta_p) A_d Q_{p\,\zeta\zeta} \\ & - \mathrm{i}2(\hat{\beta}_p/\hat{\alpha}_p - \hat{\beta}_d/\hat{\alpha}_d)\hat{\alpha}_p\hat{\alpha}_d(\sin\theta_p \sin\theta_d)\,(Q_p Q_d)_\zeta].\end{aligned} \tag{C 19}$$

It can be shown from the solutions of above equations that

$$\int_{-\infty}^{\infty} V_{\iota\,\zeta}^{(2)}\,\mathrm{d}\zeta = 0, \quad \int_{-\infty}^{\infty} W_{\iota\,\zeta\zeta}^{(2)}\,\mathrm{d}\zeta = \hat{\alpha}_\iota \int_{-\infty}^{\infty} U_{\iota\,\zeta}^{(2)}\,\mathrm{d}\zeta \quad \text{for } \iota = \{p, s, d\}, \tag{C 20}$$

$$\int_{-\infty}^{\infty} U_{J\,\zeta}^{(2)}\,\mathrm{d}\zeta = \int_{-\infty}^{\infty} V_{J\,\zeta}^{(2)}\,\mathrm{d}\zeta = \int_{-\infty}^{\infty} W_{J\,\zeta\zeta}^{(2)}\,\mathrm{d}\zeta = 0 \quad \text{for } J = \{0, 2p, p+s, p+d\}. \tag{C 21}$$

Appendix D. Nonlinear critical-layer jumps F_s and F_d

D.1. *Nonlinear critical-layer jumps when* $\lambda = O(1)$

The nonlinear critical-layer jumps F_s and F_d in (5.5) and (5.6) become, when $\lambda = O(1)$,

$$\begin{aligned}F_s(\bar{t}|A_p, A_d^*) = {} & \mu_{s1} \int_{-\infty}^{\bar{t}} \mathrm{e}^{-(1/3)\lambda\hat{\alpha}_s^2\nu^2\tau_1^3}\ \tau_1^2 A_p(\bar{t} - \nu\tau_1) A_d^*(\tilde{t}_1)\,\mathrm{d}\tilde{t}_1 \\ & + \mu_{s2} \int_{-\infty}^{\bar{t}} \int_{-\infty}^{\tilde{t}_1} \mathrm{e}^{-(1/3)\lambda\hat{\alpha}_p^2\nu^3[\hat{\nu}^2\tau_1^3 + \tau_2^3 + (\hat{\nu}\tau_1 + \tau_2)^3/\nu]} \tau_1 A_p[\bar{t} - \nu(\bar{t} - \tilde{t}_2)] A_d^*(\tilde{t}_2)\,\mathrm{d}\tilde{t}_2\,\mathrm{d}\tilde{t}_1,\end{aligned} \tag{D 1}$$

$$\begin{aligned}F_d(\bar{t}|A_p, A_s^*) = {} & \mu_{d1} \int_{-\infty}^{\bar{t}} \mathrm{e}^{-(1/3)\lambda\hat{\alpha}_s^2\nu^2\tau_1^3}\ \tau_1^2 A_p(\bar{t} - \hat{\nu}\tau_1) A_s^*(\tilde{t}_1)\,\mathrm{d}\tilde{t}_1 \\ & + \mu_{d2} \int_{-\infty}^{\bar{t}} \int_{-\infty}^{\tilde{t}_1} \mathrm{e}^{-(1/3)\lambda\hat{\alpha}_s^2\hat{\nu}[\nu^2\tau_1^3 + \tau_2^3 + (\nu\tau_1 + \tau_2)^3/\hat{\nu}]} \tau_1 A_p[\bar{t} - \hat{\nu}(\bar{t} - \tilde{t}_2)] A_s^*(\tilde{t}_2)\,\mathrm{d}\tilde{t}_2\,\mathrm{d}\tilde{t}_1,\end{aligned} \tag{D 2}$$

where

$$\tau_1 = \bar{t} - \tilde{t}_1, \quad \tau_2 = \tilde{t}_1 - \tilde{t}_2, \quad \hat{\nu} \equiv \alpha_s/\alpha_p = \hat{\alpha}_s/\hat{\alpha}_p, \quad \nu \equiv 1 - \hat{\nu} > 0, \tag{D 3}$$

$$\{\mu_{s1},\ \mu_{s2}\} = 2(\hat{\beta}_p/\hat{\alpha}_p - \hat{\beta}_d/\hat{\alpha}_d)\,\hat{\alpha}_p\nu\left\{\pi(\sin\theta_d)\nu^2\hat{\alpha}_s\hat{\gamma}_p,\ (\sin\theta_p)\mu_{s1}/(\hat{\nu}\hat{\gamma}_p)\right\}, \tag{D 4}$$

$$\{\mu_{d1},\ \mu_{d2}\} = 2\pi(\hat{\beta}_p/\hat{\alpha}_p - \hat{\beta}_s/\hat{\alpha}_s)(\nu\,\hat{\alpha}_s^2\hat{\beta}_s/\hat{\gamma}_d)\left\{\nu\,\hat{\gamma}_p,\ 2(\hat{\beta}_p/\hat{\alpha}_p - \hat{\beta}_s/\hat{\alpha}_s)(\sin\theta_p)\,\hat{\alpha}_s\right\}. \tag{D 5}$$

D.2. *Inviscid nonlinear critical-layer jumps*

By putting $\lambda = 0$ into (D 1) and (D 2), one can obtain

$$F_s(\bar{t}|A_p, A_d^*) = \mu_{si} \int_{-\infty}^{\bar{t}} (\bar{t} - \tilde{t})^2 A_p[\bar{t} - \nu(\bar{t} - \tilde{t})] A_d^*(\tilde{t})\, \mathrm{d}\tilde{t}, \tag{D 6}$$

$$F_d(\bar{t}|A_p, A_s^*) = \mu_{di} \int_{-\infty}^{\bar{t}} (\bar{t} - \tilde{t})^2 A_p[\bar{t} - \hat{\nu}(\bar{t} - \tilde{t})] A_s^*(\tilde{t})\, \mathrm{d}\tilde{t}, \tag{D 7}$$

where

$$\mu_{si} = (1 + \tan\theta_p \tan\theta_s)(\cos^2\theta_p)\mu_{s1}, \quad \mu_{di} = (1 + \tan\theta_p \tan\theta_d)(\cos^2\theta_p)\mu_{d1}. \tag{D 8}$$

D.3. *Viscous-limit nonlinear critical-layer jumps*

The asymptotic estimate of (D 1) and (D 2) in the viscous limit, as $\lambda \to \infty$, can be obtained by introducing $\tau_1 = \tilde{\tau}_1/\lambda^{1/3}$ and $\tau_2 = \tilde{\tau}_2/\lambda^{1/3}$,

$$F_s(\bar{t}|A_p, A_d^*) = (\mu_{sv}/\lambda) A_p(\bar{t}) A_d^*(\bar{t}), \quad F_d(\bar{t}|A_p, A_s^*) = (\mu_{dv}/\lambda) A_p(\bar{t}) A_s^*(\bar{t}), \tag{D 9}$$

where

$$\mu_{sv} = 2\pi(\hat{\beta}_p/\hat{\alpha}_p - \hat{\beta}_d/\hat{\alpha}_d)(\sin\theta_d)\nu[\hat{\gamma}_p/\hat{\nu} + 2(\hat{\beta}_p/\hat{\alpha}_p - \hat{\beta}_d/\hat{\alpha}_d)(\sin\theta_p)\hat{\alpha}_p^3 I_{sv}], \tag{D 10}$$

$$\mu_{dv} = 2\pi(\hat{\beta}_p/\hat{\alpha}_p - \hat{\beta}_s/\hat{\alpha}_s)(\hat{\alpha}_p\, \hat{\beta}_s/\hat{\gamma}_d)[(\hat{\gamma}_p/\hat{\alpha}_p) + 2\nu(\hat{\beta}_p/\hat{\alpha}_p - \hat{\beta}_s/\hat{\alpha}_s)(\sin\theta_p)\, \hat{\alpha}_p^2 I_{dv}], \tag{D 11}$$

$$I_{sv} = \int_0^\infty \int_0^\infty \mathrm{e}^{-(1/3)\hat{\alpha}_p^2[\hat{\nu}^2\tilde{\tau}_1^3 + \tilde{\tau}_2^3 + \nu^2\{(\tilde{\tau}_1+\tilde{\tau}_2)/\nu - \tilde{\tau}_1\}^3]}\, \tilde{\tau}_1\, \mathrm{d}\tilde{\tau}_2\, \mathrm{d}\tilde{\tau}_1, \tag{D 12}$$

$$I_{dv} = \int_0^\infty \int_0^\infty \mathrm{e}^{-(1/3)\hat{\alpha}_p^2[\nu^2\tilde{\tau}_1^3 + \tilde{\tau}_2^3 + \hat{\nu}^2\{(\tilde{\tau}_1+\tilde{\tau}_2)/\hat{\nu} - \tilde{\tau}_1\}^3]}\, \tilde{\tau}_1\, \mathrm{d}\tilde{\tau}_2\, \mathrm{d}\tilde{\tau}_1. \tag{D 13}$$

Appendix E. Derivation of amplitude equations

E.1. *Amplitude equation of the primary mode*

From (5.7) and (5.9), one can show that $D_p = 0$, as was already used in (B 1). By substituting (5.8) into the solvability equation (3.40) (with subscript p), the amplitude equation of the primary mode is derived as

$$\mathrm{d}A_p/\mathrm{d}\bar{t} = \kappa_p A_p, \quad \kappa_p = 1. \tag{E 1}$$

The primary-mode growth rate κ_p is normalized to be one by choosing $\hat{\kappa}$ and $\tilde{\zeta}_o$, introduced in (5.2), as

$$\hat{\kappa} = -\pi U_c'' c\, |b_p|^2\, \hat{\alpha}_p/[2\bar{\beta} U_c'^2\, \hat{\gamma}_p \tanh(\gamma_p H)], \quad \tilde{\zeta}_o = -U_c' R_p/(\pi U_c'' \hat{\alpha}_p\, |b_p|^2), \tag{E 2}$$

where R_p is given by (3.41) (with subscript p). The solution of (E 1) becomes $A_p = a_p \exp(\kappa_p \bar{t})$, where $a_p = 1$ if we choose t_o and X_o in (5.2), to satisfy

$$(\sqrt{M/U_c'}/\hat{\kappa}^3)\tilde{A}_p^{(o)} \mathrm{e}^{\hat{\kappa} t_o} \mathrm{e}^{\mathrm{i}\hat{\alpha}_p(X_o - \hat{\kappa} t_o \tilde{\zeta}_o)} = 1, \quad \sqrt{M} = \bar{\beta}^2 |J_s|\, |b_s|^2 (\cos\theta_s)/(\bar{\alpha}^2 \sqrt{U_c'}). \tag{E 3}$$

The $\tilde{A}_p^{(o)}$ is a non-normalized initial amplitude of $\tilde{A}_p$,

$$\tilde{A}_p = \tilde{A}_p^{(o)} \mathrm{e}^{\tilde{\kappa}_p t_1}, \quad \tilde{\kappa}_p = \tilde{A}_{p_{t_1}}/\tilde{A}_p = \bar{\alpha}\hat{\kappa} U_c'(1 - \mathrm{i}\hat{\alpha}_p \tilde{\zeta}_o), \tag{E 4}$$

where $\tilde{\kappa}_p$ is the non-normalized linear growth rate of the primary mode.

It is assumed that

$$U_c'' < 0 \quad \text{and} \quad U_c' > 0, \tag{E 5}$$

according to Fjørtoft's theorem (Drazin & Reid 2004). The linear growth rate in (6.5) is positive and the real constants $\hat{\kappa}$ and M in (E 2) and (E 3) are positive.

E.2. *Amplitude equation of the secondary mode*

The solvability equation (3.40) with (5.2), (5.8), (5.10) and (E 2) becomes

$$\mathrm{d}B_s/\mathrm{d}\bar{t} = (\kappa_s/b_s)A_s - \chi_s J_s D_s B_s, \tag{E 6}$$

where

$$\kappa_s = \frac{|b_s|^2\,\hat{\alpha}_s\hat{\gamma}_p\tanh(\gamma_p H)}{|b_p|^2\,\hat{\alpha}_p\hat{\gamma}_s\tanh(\gamma_s H)}\left[1+\frac{\mathrm{i}U_c'}{\pi U_c''\,|b_s|^2}\left\{R_s - R_p\frac{\hat{\gamma}_s\tanh(\gamma_s H)}{\hat{\gamma}_p\tanh(\gamma_p H)}\right\}\right], \tag{E 7}$$

$$\chi_s = \kappa_s + \mathrm{i}U_c'\hat{\alpha}_s\hat{\gamma}_p\tanh(\gamma_p H)/[\pi U_c'' J_s|b_p\,|^2\,\hat{\alpha}_p\hat{\gamma}_s\tanh(\gamma_s H)]. \tag{E 8}$$

By differentiating the first equation in (5.10) with respect to $\bar{t}$, we obtain

$$\mathrm{d}A_s/\mathrm{d}\bar{t} = b_s[\mathrm{d}B_s/\mathrm{d}\bar{t} + J_s\,\mathrm{d}(D_s B_s)/\mathrm{d}\bar{t}]. \tag{E 9}$$

The secondary-mode amplitude equation is derived by substituting (E 6) into (E 9), and replacing $D_s B_s$ in the resulting equation by (5.9),

$$\mathrm{d}\bar{A}_s/\mathrm{d}\bar{t} = \kappa_s\bar{A}_s + \varphi_s(\chi_s\bar{F}_s - \mathrm{d}\bar{F}_s/\mathrm{d}\bar{t}), \tag{E 10}$$

where we have put

$$\bar{A}_s = A_s/a_s, \quad \bar{A}_d = A_d/a_s^*, \quad \bar{F}_s \equiv F_s(\bar{t}|A_p, \bar{A}_d^*) = F_s(\bar{t}|A_p, A_d^*)/a_s, \tag{E 11}$$

with F_s given in (D 1), (D 6) and (D 9). If the normalization parameter M is chosen as in (E 3), the complex coefficient φ_s becomes

$$\varphi_s = J_s b_s^2/(|J_s|\,|b_s|^2). \tag{E 12}$$

The integro-differential equation (E 10) is solved subject to the initial condition

$$\bar{A}_s = A_s/a_s \to \mathrm{e}^{\kappa_s\bar{t}} \quad \text{as } \bar{t}\to-\infty, \tag{E 13}$$

where a_s is proportional to the ratio of non-normalized initial amplitudes of the secondary to primary modes,

$$a_s = (\tilde{A}_s^{(o)}/\tilde{A}_p^{(o)})\,\mathrm{e}^{-(1-\kappa_s)\hat{\kappa}t_o - \mathrm{i}(\hat{\alpha}_p-\hat{\alpha}_s)(X_o-\hat{\kappa}t_o\tilde{\xi}_o)}, \tag{E 14}$$

with $\tilde{A}_p^{(o)}$ defined by (E 4) and $\tilde{A}_s^{(o)}$, by

$$\tilde{A}_s \to \tilde{A}_s^{(o)}\mathrm{e}^{\tilde{\kappa}_s t_1} \quad \text{as } t_1\to-\infty. \tag{E 15}$$

The non-normalized linear growth rate of the secondary mode, $\tilde{\kappa}_s$, becomes

$$\tilde{\kappa}_s = \lim_{t_1\to-\infty}(\mathrm{d}\tilde{A}_s/\mathrm{d}t_1)/\tilde{A}_s = \lim_{t_1\to-\infty}(\mathrm{d}\tilde{B}_s/\mathrm{d}t_1)/\tilde{B}_s = \bar{\alpha}\hat{\kappa}\,U_c'(\kappa_s - \mathrm{i}\hat{\alpha}_s\tilde{\zeta}_o). \tag{E 16}$$

E.3. *Amplitude equation of the difference mode*

The amplitude equation of the nonlinearly generated difference mode is obtained from (5.9), (5.10) with (3.46) and (E 11) as

$$\bar{A}_d = -\varphi_d\bar{F}_d, \tag{E 17}$$

where

$$\bar{F}_d \equiv F_d(\bar{t}|A_p, \bar{A}_s^*) = F_d(\bar{t}|A_p, A_s^*)/a_s^*, \tag{E 18}$$

with F_d given in (D 2), (D 7) and (D 9), and

$$\varphi_d = J_d b_d^2/(|J_s|\,|b_s|^2). \tag{E 19}$$

Appendix F. Special solutions of amplitude equations

F.1. *When* $\theta_s = \theta_p - \pi/2$ *and* $\lambda = 0$

From (D 8), one can show that μ_{si}, which appears in the inviscid secondary-mode amplitude equation (5.14), becomes zero when $\theta_s = \theta_p - \pi/2$. In this special case, the secondary mode grows exponentially without a nonlinear contribution. The difference mode also grows exponentially due to the nonlinear coupling between the linear primary and secondary modes. With the constraint (3.5) for the $2+1$ mode interaction, the amplitudes become

$$A_s = a_s \mathrm{e}^{\kappa_s \bar{t}}, \quad A_d = a_s^* a_d \mathrm{e}^{(1+\kappa_s^*)\bar{t}} \quad \text{if } \theta_s = \theta_p - \pi/2,\ \theta_p > \pi/4,\ \lambda = 0. \tag{F 1}$$

F.2. *Two-dimensional secondary wave with* $\theta_s = 0$

When the secondary mode is located at S_o in figures 3 (or 4*a*), it is a two-dimensional wave propagating in the streamwise direction of wind ($\theta_s = 0°$ and $\hat{\beta}_s = 0$). The μ_{d1}, μ_{d2}, μ_{di} and μ_{dv} in (D 5), (D 8) and (D 11) become zero if $\theta_s = 0$. As a result, the difference-mode amplitude becomes zero independently of λ, and the secondary mode continues to grow exponentially:

$$A_d = 0, \quad A_s = a_s\, \mathrm{e}^{\kappa_s \bar{t}} \quad \text{if } \theta_s = 0. \tag{F 2}$$

We can confirm that there is no nonlinear critical-layer jump for the difference mode, from (5.6),

$$(\cos\theta_s/\cos\theta_d)\, F_d(\bar{t}|A_p, A_s^*) = 0 \quad \text{if } \theta_s = 0. \tag{F 3}$$

The above result can also be proved by directly analysing the critical-layer interaction between a two-dimensional and an oblique mode of the same wave speed c. If the streamwise and spanwise wavenumbers are denoted by $(\alpha_{2D}, 0)$ and $(\alpha_{3D}, \beta_{3D})$ for the two-dimensional and oblique modes, respectively, the nonlinear critical-layer interaction produces a difference mode whose wavenumbers are $(\alpha_{2D} - \alpha_{3D}, -\beta_{3D})$ inside the critical layer. We can show that its velocity jump across the critical layer becomes zero if $\alpha_{2D} < \alpha_{3D}$ as in the present wind–wave interaction analysis, but it becomes non-zero if $\alpha_{2D} > \alpha_{3D}$, as in Wu & Stewart (1996) for the Rayleigh instability waves in shear flows.

Appendix G. g_{n-1} and h_n in (5.25) and (5.26) for $\lambda \neq 0$, and $\hat{a}_s$ and $\hat{a}_d$ in (5.28)

$$g_{n-1} = \frac{(2n+\kappa_s+\nu-1)^3\,(2n+\kappa_s-\nu-1)^3}{4\mu_{si}\mu_{di}}[I_1(n)+I_2(n)] \times [I_3^*(n-1)+I_4^*(n-1)] \quad \text{if } \lambda \neq 0, \tag{G 1}$$

$$h_n = \frac{1}{2}\,(2n+\kappa_s^*-\nu+1)^3\,[I_3(n)+I_4(n)]\,/\mu_{di} \quad \text{if } \lambda \neq 0, \tag{G 2}$$

where

$$I_1(n) = \mu_{s1} \int_0^\infty \mathrm{e}^{-(1/3)\lambda\hat{a}_s^2\nu^2\tilde{\tau}_1^3}\, \mathrm{e}^{-(2n+\kappa_s-\hat{\nu})\tilde{\tau}_1}\ \tilde{\tau}_1^2\, \mathrm{d}\tilde{\tau}_1, \tag{G 3}$$

$$I_2(n) = \mu_{s2} \int_0^\infty \int_0^\infty \mathrm{e}^{-(1/3)\lambda\hat{a}_p^2\nu^3[\hat{\nu}^2\tilde{\tau}_1^3+\tilde{\tau}_2^3+(\hat{\nu}\tilde{\tau}_1+\tilde{\tau}_2)^3\,/\nu]}\, \mathrm{e}^{-(2n+\kappa_s-\hat{\nu})(\tilde{\tau}_1+\tilde{\tau}_2)}\ \tilde{\tau}_1\, \mathrm{d}\tilde{\tau}_2\, \mathrm{d}\tilde{\tau}_1, \tag{G 4}$$

$$I_3(n) = \mu_{d1} \int_0^\infty \mathrm{e}^{-(1/3)\lambda\hat{a}_s^2\nu^2\tilde{\tau}_1^3}\, \mathrm{e}^{-(2n+\kappa_s^*+\hat{\nu})\tilde{\tau}_1}\ \tilde{\tau}_1^2\, \mathrm{d}\tilde{\tau}_1, \tag{G 5}$$

$$I_4(n) = \mu_{d2} \int_0^\infty \int_0^\infty \mathrm{e}^{-(1/3)\lambda\hat{a}_s^2\hat{\nu}[\nu^2\tilde{\tau}_1^3+\tilde{\tau}_2^3+\{\nu\tilde{\tau}_1+\tilde{\tau}_2\}^3\,/\hat{\nu}]}\, \mathrm{e}^{-(2n+\kappa_s^*+\hat{\nu})(\tilde{\tau}_1+\tilde{\tau}_2)}\ \tilde{\tau}_1\, \mathrm{d}\tilde{\tau}_2\, \mathrm{d}\tilde{\tau}_1, \tag{G 6}$$

$$\hat{a}_s = \frac{a_s \left\{ \Gamma\left[\frac{1}{2}(\kappa_s-\hat{\nu})+1\right] \Gamma\left[\frac{1}{2}(\kappa_s+\hat{\nu})\right] \right\}^3 \left(\frac{1}{16}\mu_{si}\mu_{di}\varphi_s\varphi_d^* \right)^{(1-5\kappa_s-\chi_s)/12}}{8\sqrt{3}\ \pi^{5/2}\, \Gamma\left[\frac{1}{2}(\kappa_s-\chi_s)+1\right]} \prod_{m=1}^{\infty} g_{m-1}, \tag{G 7}$$

$$\hat{a}_d = -2\pi\hat{\nu}^3 \left[\mu_{di}\varphi_d/(\mu_{si}\varphi_s^*)\right]^{1/2}. \tag{G 8}$$

Appendix H. Linear growth rate from numerical solution

The Rayleigh equation (3.12), with subscripts p for the primary wave, is solved subject to the boundary conditions

$$\Phi_p \to 0 \quad \text{as } z \to \infty, \tag{H 1}$$

$$\Phi_p = \mathrm{i}\tanh(\gamma_p H) \quad \text{at } z = 0, \tag{H 2}$$

$$\left\{ \frac{\gamma_p \hat{c}_p^2}{\tanh(\gamma_p H)} - G(\sec^2\theta_p) \right\} \Phi_p - \sigma \left\{ \hat{c}_p^2\, \partial_z\Phi_p + \hat{c}_p U_0' \Phi_p - G(\sec^2\theta_p)\Phi_p \right\} = 0 \quad \text{at } z = 0. \tag{H 3}$$

The interface condition (H 2) is obtained from (3.19) with (3.20) (with subscript p), and the other condition (H 3) can be derived by combining (3.17) with (3.13) and (3.20).

With a given γ_p and $U(z)$, (3.12) is numerically integrated from $z = \infty$, with $\Phi_p = \exp(-\gamma_p z)$, to a matching point $z = z_m$ by using the Fehlberg fourth/fifth-order Runge–Kutta scheme (Fehlberg 1970; Forsythe, Malcolm & Moler 1977) with a guessed $\hat{c}_p$, and from $z = 0$, with (H 2) and (H 3), to $z = z_m$. This process is repeated with a corrected $\hat{c}_p$ until $\partial_z\Phi_p/\Phi_p$ is matched at $z = z_m$. When the growth rate is relatively large, one can integrate on the real axis with $z_m = z_c$, for example. For a small growth rate, a complex contour path that half-circles the singularity in the lower half-plane is used (Lin 1945).

REFERENCES

Alexakis, A., Calder, A. C., Dursi, L. J., Rosner, R., Truran, J. W., Fryxell, B., Zingale, M., Timmes, F. X., Olson, K. & Ricker, P. 2004*a* On the nonlinear evolution of wind-driven gravity waves. *Phys. Fluids* **16**, 3256–3268.

Alexakis, A., Young, Y. & Rosner, R. 2002 Shear instability of fluid interfaces: stability analysis. *Phys. Rev.* E **63**, 026313.

Alexakis, A., Young, Y.-N. & Rosner, R. 2004*b* Weakly nonlinear analysis of wind-driven gravity waves. *J. Fluid Mech.* **503**, 171–200.

BENNEY, D. J. & BERGERON, R. F. JR. 1969 A new class of nonlinear waves in parallel flows. *Stud. Appl. Math.* **48**, 181–204.

BLENNERHASSETT, P. J. 1980 On the generation of waves by wind. *Phil. Trans. R. Soc. Lond.* A **298**, 451–494.

CAULLIEZ, G. & COLLARD, F. 1999 Three-dimensional evolution of wind waves from gravity-capillary to short gravity range. *Eur. J. Mech.* B **18**, 389–402.

CAVALERI, L. *et al*. 2007 Wave modelling: the state of the art. *Prog. Oceanogr.* **75**, 603–674.

CHARNOCK, H. 1955 Wind stress on a water surface. *Q. J. R. Meteorol. Soc.* **81**, 639–640.

CONTE, S. D. & MILES, J. W. 1959 On the numerical integration of the Orr–Sommerfeld equation. *J. Soc. Ind. Appl. Math.* **7**, 361–366.

DAVIS, R. E. 1969 On the high Reynolds number flow over a wavy boundary. *J. Fluid Mech.* **36**, 337–346.

DRAZIN, P. G. & REID, W. H. 2004 *Hydrodynamic Stability*, second edition. Cambridge University Press.

FEHLBERG, E. 1970 Klassiche Runge–Kutta-Formeln vierter und niedrigerer Ordnung mit Schrittweiten-Kontrolle und ihre Anwendung auf Wärmeleitungsprobleme. *Computing* **6**, 61–71.

FORSYTHE, G. E, MALCOLM, M. A. & MOLER, C. B. 1977 *Computer Methods for Mathematical Computations*. Prentice Hall.

GOLDSTEIN, M. E. 1995 The role of nonlinear critical layers in boundary layer transition. *Phil. Trans. R. Soc. Lond.* A **352**, 425–442.

GOLDSTEIN, M. E. & CHOI, S. W. 1989 Nonlinear evolution of interacting oblique waves on two-dimensional shear layers. *J. Fluid Mech.* **207**, 97–120. Also Corrigendum, *J. Fluid Mech.***216**, 659–663.

GOLDSTEIN, M. E., DURBIN, P. A. & LEIB, S. J. 1987 Roll-up of vorticity in adverse-pressure-gradient boundary layers. *J. Fluid Mech.* **183**, 325–342.

GOLDSTEIN, M. E. & HULTGREN, L. S. 1988 Nonlinear spatial evolution of an externally excited instability wave in a free shear layer. *J. Fluid Mech.* **197**, 295–330.

GOLDSTEIN, M. E. & LEE, S. S. 1992 Fully coupled resonant-triad interaction in an adverse-pressure-gradient boundary layer. *J. Fluid Mech.* **245**, 523–551.

GOLDSTEIN, M. E. & LEE, S. S. 1993 Oblique instability waves in nearly parallel shear flows. In *Nonlinear Waves and Weak Turbulence with Applications in Oceanography and Condensed Matter Physics* (ed. N. Fitzmaurice, D. Gurarie, F. McCaughan & W. Woyczynski). pp. 159–177. Birkhäuser.

GOLDSTEIN, M. E. & LEIB, S. J. 1989 Nonlinear evolution of oblique waves on compressible shear layers. *J. Fluid Mech.* **207**, 73–96.

HRISTOV, T. S., MILLER, S. D. & FRIEHE, C. A. 2003 Dynamical coupling of wind and ocean waves through wave-induced air flow. *Nature* **442**, 55–58.

HULTGREN, L. S. 1992 Nonlinear spatial equilibration of an externally excited instability wave in a free shear layer. *J. Fluid Mech.* **236**, 635–664.

JANSSEN, P. 2004 *The Interaction of Ocean Waves and Wind*. Cambridge University Press.

KINSMAN, B. 1965 *Wind Waves, Their Generation and Propagation on the Ocean Surface*. Prentice Hall.

KOMEN, G. J., CAVALERI, L., DONELAN, M., HASSELMANN, K., HASSELMANN, S. & JANSSEN, P. A. E. M. 1994 *Dynamics and Modelling of Ocean Waves*. Cambridge University Press.

LEE, S. S. 1997 Generalized critical-layer analysis of fully coupled resonant-triad interactions in boundary layers. *J. Fluid Mech.* **347**, 71–103.

LEE, S. S. & WUNDROW, D. W. 2011 Transition from long-crested to short-crested seas by wind–wave interaction. In *Proceedings of the 21st International Offshore (Ocean) & Polar Engineering Conference, June 19-24, 2011, Maui, HI*, vol. 3, pp. 298–305. ISOPE.

LIN, C. C. 1945 On the stability of two-dimensional parallel flows. Parts 1, 2, 3. *Q. Appl. Math.* **3**, 117–142 218–234, 277–301.

MILES, J. W. 1957 On the generation of surface waves by shear flows. *J. Fluid Mech.* **3**, 185–204.

MILES, J. W. 1993 Surface-wave generation revisited. *J. Fluid Mech.* **256**, 427–441.

MILES, J. W. 1997 Generation of surface waves by wind. *Appl. Mech. Rev.* **50**, R5-9.

MORLAND, L. C. & SAFFMAN, P. G. 1993 Effect of wind profile on the instability of wind blowing over water. *J. Fluid Mech.* **252**, 383–398.

NAYFEH, A. H. 1981 *Introduction to Perturbation Techniques*. Wiley.

PHILLIPS, O. M. 1960 On the dynamics of unsteady gravity waves of finite amplitude. Part 1. The elementary interactions. *J. Fluid Mech.* **9**, 193–217.

REUTOV, V. P. 1980 The plasma-hydrodynamic analogy and the nonlinear stage of instability of wind waves. *Izv. Atmos. Ocean. Phys.* **16**, 938–943.

SULLIVAN, P. P. & MCWILLIAMS, J. C. 2010 Dynamics of winds and currents coupled to surface waves. *Annu. Rev. Fluid Mech.* **42**, 19–42.

VALENZUELA, G. R. 1976 The growth of gravity-capillary waves in a coupled shear flow. *J. Fluid Mech.* **76**, 229–250.

WEHAUSEN, J. V. & LAITONE, E. V. 1960 *Surface Waves* (ed. W. Flügge & C. Truesdell). *Handbuch der Physik*, IX, pp. 446–778. Springer.

WU, X. 1992 The nonlinear evolution of high-frequency resonant-triad waves in an oscillatory Stokes layer at high Reynolds number. *J. Fluid Mech.* **245**, 553–597.

WU, X., LEE, S. S. & COWLEY, S. J. 1993 On the weakly nonlinear three-dimensional instability of shear layers to pairs of oblique waves: the Stokes layer as a paradigm. *J. Fluid Mech.* **253**, 681–721.

WU, X. & STEWART, P. A. 1996 Interaction of phase-locked modes: a new mechanism for the rapid growth of three-dimensional disturbances. *J. Fluid Mech.* **316**, 335–372.

WU, X., STEWART, P. A. & COWLEY, S. J 2007 On the catalytic role of the phase-locked interaction of Tollmien–Schlichting waves in boundary-layer transition. *J. Fluid Mech.* **590**, 265–294.

WUNDROW, D. W., HULTGREN, L. S. & GOLDSTEIN, M. E. 1994 Interaction of oblique instability waves with a nonlinear plane wave. *J. Fluid Mech.* **264**, 343–372.